

ELECTRICAL

FACILITY FORM 602

N 68-26175

(ACCESSION NUMBER) 65 (THRU) 1

(PAGES) CR 61833 (CODE) 14

(NASA CR OR TMX OR AD NUMBER) (CATEGORY)

An Analysis Of A Single Axis Platform

PREPARED BY
ADVANCED STUDIES GROUP
AUBURN UNIVERSITY
J. L. LOWRY, PROJECT LEADER

653 July 65

Microfiche (MF)

Hard copy (HC)

CFSTI PRICE(S) \$

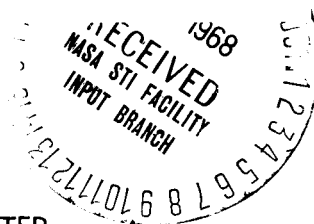
GPO PRICE \$

3.00
65

TECHNICAL REPORT
DECEMBER 1966

CONTRACT—NAS 8-20004

GEORGE C. MARSHALL SPACE FLIGHT CENTER
NATIONAL AERONAUTICS & SPACE ADMINISTRATION
HUNTSVILLE, ALABAMA 35812



AUBURN RESEARCH FOUNDATION
AUBURN UNIVERSITY
AUBURN, ALABAMA

RQ7-5

ERRATA SHEET
FOR
AN ANALYSIS OF A SINGLE AXIS PLATFORM

TECHNICAL REPORT

December, 1966

BY

James L. Lowry

CONTRACT NAS8-20004

GEORGE C. MARSHALL SPACE FLIGHT CENTER
NATIONAL AERONAUTICS AND SPACE ADMINISTRATION
HUNTSVILLE, ALABAMA

ERRATA SHEET

For

AN ANALYSIS OF A SINGLE AXIS PLATFORM

Item 1

Page 49 - Equation (V-2) should read:

$$\frac{\theta_1(s)}{L_{yge}(s)} = \frac{1}{I_{yg} + I_{yf}} \cdot \frac{D(H)S}{\prod (S-P_i)}$$

Item 2

Page 50 - Equation (V-4) should read:

$$\theta_1(s) = \frac{-\omega_{yc}(s)}{s} +$$

$$\frac{\frac{1}{I_{yg} + I_{yf}} \left\{ L_{yge}(s) D(H)S - \frac{L_{zf}(s) H_w D(H)}{I_{zf}} - \frac{L_{zf}(s) K_2 N(H)}{S I_{zf}} \right\}}{\prod (S-P_i)}$$

Item 3

Page 50 - Equation (V-6) should read:

$$\frac{\theta_1(s)}{L_{yge}(s)} = \frac{5 \times 10^{-5} s(s+1)(s+6000)(s+1500+j1000)(s+1500-j1000)}{\prod_{i=1}^7 (S-P_i)}$$

Item 4

Page 53 - Equation (VI-2) should read:

$$\theta_1(t) = -W_{yc}t - 40.2 \times 10^{-8}t L_z - 49.4 \times 10^{-12}L_z + 80.4 \times 10^{-5}W_{zg} + \sum_{i=1}^7 K_i e^{p_i t}$$

1

AN ANALYSIS OF A
SINGLE AXIS PLATFORM

Prepared by
ADVANCED STUDIES GROUP
AUBURN UNIVERSITY

J. L. Lowry, Project Leader

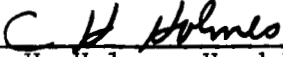
TECHNICAL REPORT

December, 1966

Contract-NAS8-20004

George C. Marshall Space Flight Center
National Aeronautics and Space Administration
Huntsville, Alabama 35812

APPROVED BY:


C. H. Holmes, Head Professor
Electrical Engineering
Department

SUBMITTED BY:

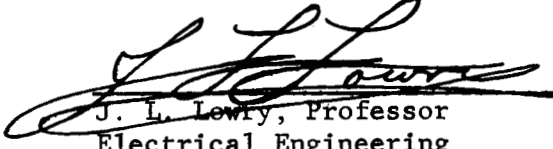

J. L. Lowry, Professor
Electrical Engineering
Department

TABLE OF CONTENTS

LIST OF SYMBOLS.....	iv
LIST OF FIGURES.....	vi
FOREWORD.....	vii
SUMMARY.....	viii
PERSONNEL	ix
I. INTRODUCTION.....	1
A. Definition and Behavior of a Gyroscope	1
B. Definition and Operation of an Ideal Single Axis Platform.....	5
II. DERIVATION OF EQUATIONS OF MOTION OF AN IDEAL SAP.....	10
A. Introduction.....	10
B. Derivation of the Float Torque Equation.....	17
C. Derivation of the Gimbal Torque Equation	19
D. Derivation of the Block Diagram of an Ideal SAP.....	22
III. DERIVATION OF THE EQUATIONS OF MOTION OF AN IDEAL SAP WHEN THE TORSIONAL STIFFNESS OF THE GAS BEARING BETWEEN THE GIMBAL AND FLOAT IS CONSIDERED	29
IV. STABILITY ANALYSIS.....	37
A. Introduction.....	37
B. Stability of an Ideal SAP with Infinite Torsional Stiffness of the Gas Bearing	39
C. Stability of an Ideal SAP with Finite Torsional Stiffness of the Gas Bearing.....	42
V. ANALYSIS OF AN IDEAL SAP.....	48

A.	Introduction.....	48
B.	Transfer Function of an Ideal SAP with Infinite Torsional Stiffness of the Gas Bearing.....	49
C.	Reaction of the Ideal SAP to Angular Rates Perpendicular to Its Reference Axis.....	51
VI.	CONCLUSION.....	53
	REFERENCES.....	56

LIST OF SYMBOLS

SYMBOL	DEFINITION
SAP	<u>Single Axis Platform.</u>
SAR	<u>Single Axis Reference.</u>
IA	Input axis of SAP.
OA	Output axis of SAP.
SA	Spin axis of SAP
Δ	The "delta" shall mean an incremental change in that quantity when placed before the quantity.
-	The "bar" shall mean a vector quantity when placed over the quantity.
.	The "dot" shall mean a time derivative of a quantity when placed over the quantity.
x	The "x" shall mean a scalar derivative when placed above a quantity.
x,y,z	The axis of a right-hand orthogonal coordinate system. When used as a subscript of a quantity, the subscript shall mean that component of the quantity along that axis.
c,g,f,w,gi	These letters refer to a particular coordinate system when used as a subscript c-case coordinate system g-gimbal coordinate system f-float coordinate system w-wheel coordinate system gi-inner gimbal coordinate system.
$\bar{i}, \bar{j}, \bar{k}$	Unit vector along the x,y, and z axis respectively.
H	Angular momentum

SYMBOL	DEFINITION
L	Torque
F	Force
θ_1	The angle between the gimbal and case.
θ_2	The angle between the float and gimbal.
C	Three by three transformation matrix relating two coordinate systems.
ω	Angular velocity.
K_2	Feedback gain.
$H(s)$	Feedback transfer function.
I	Tensor of inertia.
ω_s	Angular velocity of the wheel with respect to the float.
K_b	Torsional stiffness constant.

LIST OF FIGURES

1. A Cardan suspension.....	2
2. Precession of a spinning flywheel.....	3
3. Vector illustration of precession.....	4
4. Simplified SAP.....	7
5. Functional sketch of an ideal SAP.....	11
6. Elementary block diagram of the SAP showing input- output relationships.....	13
7. Signal flow graph of an ideal floated gimballed gyroscope.....	26
8. Signal flow graph of an ideal SAP.....	27
9. Block diagram of an ideal SAP.....	28
10. Functional sketch of an ideal SAP with a finite torsional stiffness gas bearing.....	30
11. Signal flow graph of an ideal floated gimballed gyroscope with a finite torsional stiffness gas bearing...	33
12. Signal flow graph of an ideal SAP with a finite torsional stiffness gas bearing.....	35
13. Block diagram of an ideal SAP with a finite torsional stiffness gas bearing.....	36
14. Simplified block diagram of the SAP for stability analysis.....	38
15. Root locus of the ideal SAP.....	41
16. Open-loop Bode plot of the ideal SAP.....	43
17. Root locus of the ideal SAP when the finite torsional stiffness of the gas bearing is considered.....	46

FOREWORD

This is a technical report prepared by the Advanced Studies Group, Electrical Engineering Department, Auburn University, toward fulfillment of Contract NAS8-20004 granted to Auburn Research Foundation, Auburn, Alabama. This contract was originally awarded January 19, 1965, and was extended to January 18, 1966. It was further extended to April 18, 1966, and thereafter to December 18, 1966.

SUMMARY

The principles of operation of the gyroscope and the ideal Single Axis Platform (SAP) are reviewed in Chapter I. In Chapter II the equations of motion of an ideal SAP are derived and a signal flow graph and a block diagram are constructed from the equations of motion. The equations of motion of an ideal SAP, when the torsional stiffness of the gas bearing between the float and gimbal is considered, are presented in Chapter III, and a signal flow graph and a block diagram are constructed from these equations of motion. A discussion of the stability of the ideal SAP with finite and infinite torsional stiffness of the gas bearing is presented in Chapter IV. The analysis of an ideal SAP for various inputs are presented in Chapter V. Chapter VI is the conclusion of this study.

PERSONNEL

The following staff members of Auburn University have actively contributed in this study.

J. L. Lowry	-Professor of Electrical Engineering Project Leader-October 19, 1965 to Present.
S. N. James	-Assistant Professor of Electrical Engineering 1/3 time-September 1, 1966 to Present.
C. L. Connor	-Graduate Assistant in Electrical Engineering 2/3 time-September 1, 1965 to September 1, 1966.
D. W. Kelly	-Graduate Assistant in Electrical Engineering Full Time-January 19, 1965 to Present.
T. L. Richards	-Graduate Assistant in Electrical Engineering 2/3 time-June 1, 1966 to Present.

I. INTRODUCTION [1,2,3]

A. Definition and Behavior of a Gyroscope

A gyroscope may be broadly defined as a body rotating at a high angular velocity about an axis which is called its spin axis. The usual form of a gyroscope is a mechanical device of which the essential part is a heavy flywheel mounted such that, while spinning at high speed, its axis of rotation can turn in any direction about a fixed point on the axis of rotation. The flywheel, mounted so as to turn about its center of gravity by means of double gimbals, is shown in Figure 1. This arrangement is called a Cardan suspension.

For the sake of explanation, the spinning flywheel may be represented as shown in Figure 2. This spinning flywheel has the property of resisting any effort to change the direction of its spin axis. For example, if the spin axis is along the X-axis as shown and a steady force-couple or torque is applied about the Y-axis, perpendicular to the spin axis, the spinning flywheel will not rotate around the Y-axis as would be expected, but will rotate around the Z-axis. This rotation of the spin axis about the Z-axis is called "precession," and is a consequence of the fundamental relation

$$\frac{d\bar{H}}{dt} = \bar{L} \quad . \quad ^* \quad (I-1)$$

*Where a bar "-" indicates a vector.

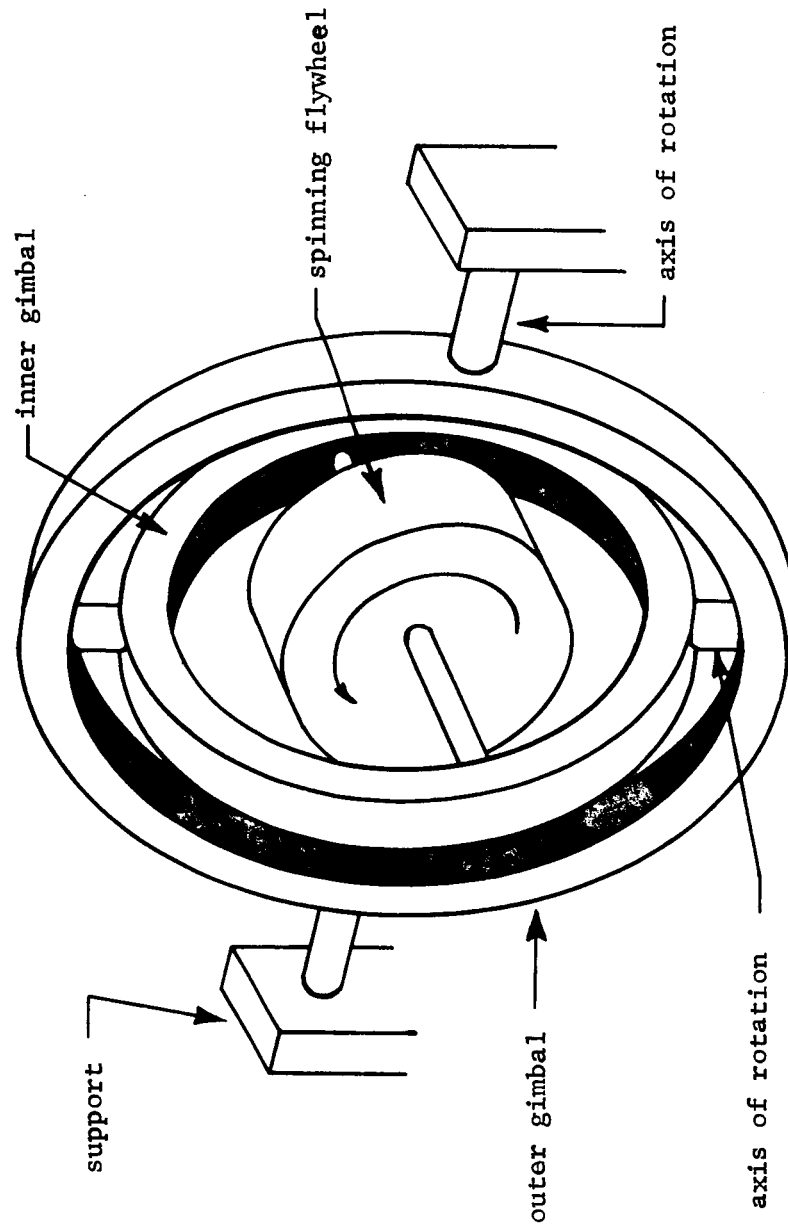


Fig. 1--A Cardan suspension.

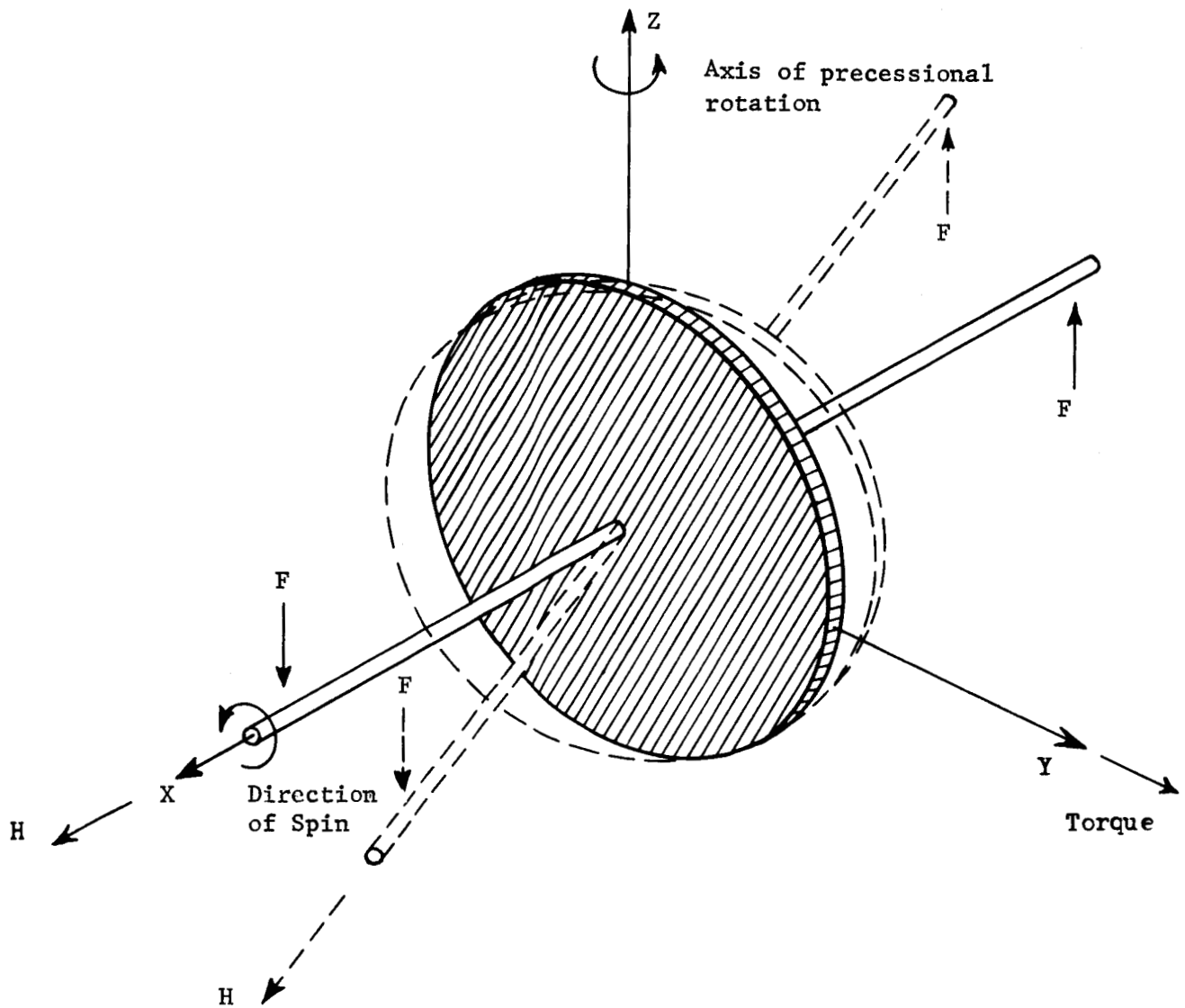


Fig. 2--Precession of a spinning flywheel.

Equation (I-1) shows that the applied torque \bar{L} is equal to the rate of change in angular momentum \bar{H} of the spinning flywheel.

To illustrate precession assume that a constant torque is applied to the spinning flywheel shown in Figure 2 for an incremental time interval Δt . According to Equation (I-1), the incremental change in \bar{H} , $\Delta\bar{H}$, will be

$$\Delta\bar{H} = \bar{L} \Delta t, \quad (\text{I-2})$$

where the direction of $\Delta\bar{H}$ is along the torque vector \bar{L} . If the torque vector \bar{L} is perpendicular to the spin axis of the body, the \bar{H} vector will add with $\Delta\bar{H}$ as shown in Figure 3 to give the resulting angular momentum of the flywheel.

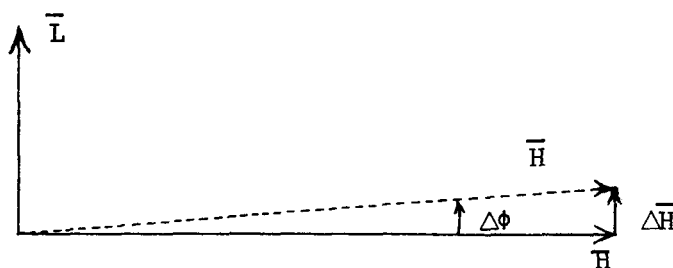


Fig. 3--Vector illustration of precession.

Therefore, in effect, the \bar{H} vector has rotated about an axis perpendicular to both the torque vector and the spin axis an amount $\Delta\phi$. If H is large with respect to ΔH , the incremental angle $\Delta\phi$ is given by $H\Delta\phi \approx \Delta H$. Since $\Delta\bar{H} = \bar{L} \Delta t$, $\omega \equiv \Delta\phi/\Delta t \approx L/H$, where ω is the magnitude of the precession

rate vector. The precession rate vector is directed perpendicular to the plane containing \bar{L} and \bar{H} , and in the direction that a right handed screw would move if rotated from \bar{H} to \bar{L} . The spin axis (\bar{H} vector) will always tend to align itself with the applied torque (\bar{L} vector).

B. Definition and Operation of an Ideal Single Axis Platform

The Single Axis Platform (SAP) is a device that measures angular rotation of its outer case about a single reference axis through the center of the device. The SAP is sometimes called a Single Axis Reference (SAR), a name more descriptive of its actual performance. The SAP maintains its reference axis along one of the axes of its case by using a floated gimballed gyroscope in conjunction with a closed-loop feedback control system. The reference axis of the SAP will rotate with the case for all angular rate vector components perpendicular to the reference axis. The angular displacement of the case about the reference axis is the integral of the rate vector component along the reference axis. The output of the SAP is obtained from an encoder that measures the angular rotation of the case about the reference axis, and consists of an electrical pulse every time the angle changes by $\Delta\phi$ arc seconds. These output pulses may be summed, with the correct sign, and multiplied by $\Delta\phi$ to give the total angular rotation, or they may be summed over a time interval Δt and this sum used to calculate the angular rate of the case about its reference

axis. This angular rate is the magnitude of the component along the reference axis of the total angular rate vector of the case of the SAP. If three SAP's are mounted on a vehicle so that their reference axes are non-planar, the three components of the angular rate vector along the three reference axes of the SAP's can be used to calculate the angular rate vector of the vehicle.

The SAP's construction is shown in Figure 4, and is centered around the gyro wheel, or rotor. The gyro wheel, due to its almost constant, high angular momentum, establishes the gyroscopic effect. The gyro wheel is bearing mounted to, and is sealed inside of, the inner cylinder of the SAP. The inner cylinder of the SAP is suspended in an almost frictionless gas bearing inside the outer cylinder* of the SAP. The outer cylinder is mounted by trunnion bearings to the case, and is free to turn about the input reference axis IA (see Figure 4). A null position pickoff device is mounted to the outer cylinder and is positioned so that it is sensitive to angular displacements of the inner cylinder with respect to a predetermined null position between the inner and outer cylinders. A torque motor (torquer) is mounted in the case and can torque the outer cylinder about IA, producing a torque vector along IA. Also mounted along IA is an encoder, a device that measures the relative angular displacement between the case and the outer cylinder.

To understand the operation of an ideal SAP, consider its reaction to angular motion of the housing about the three axes, IA, OA, and

*The inner cylinder and outer cylinder are referred to as the float and gimbal respectively.

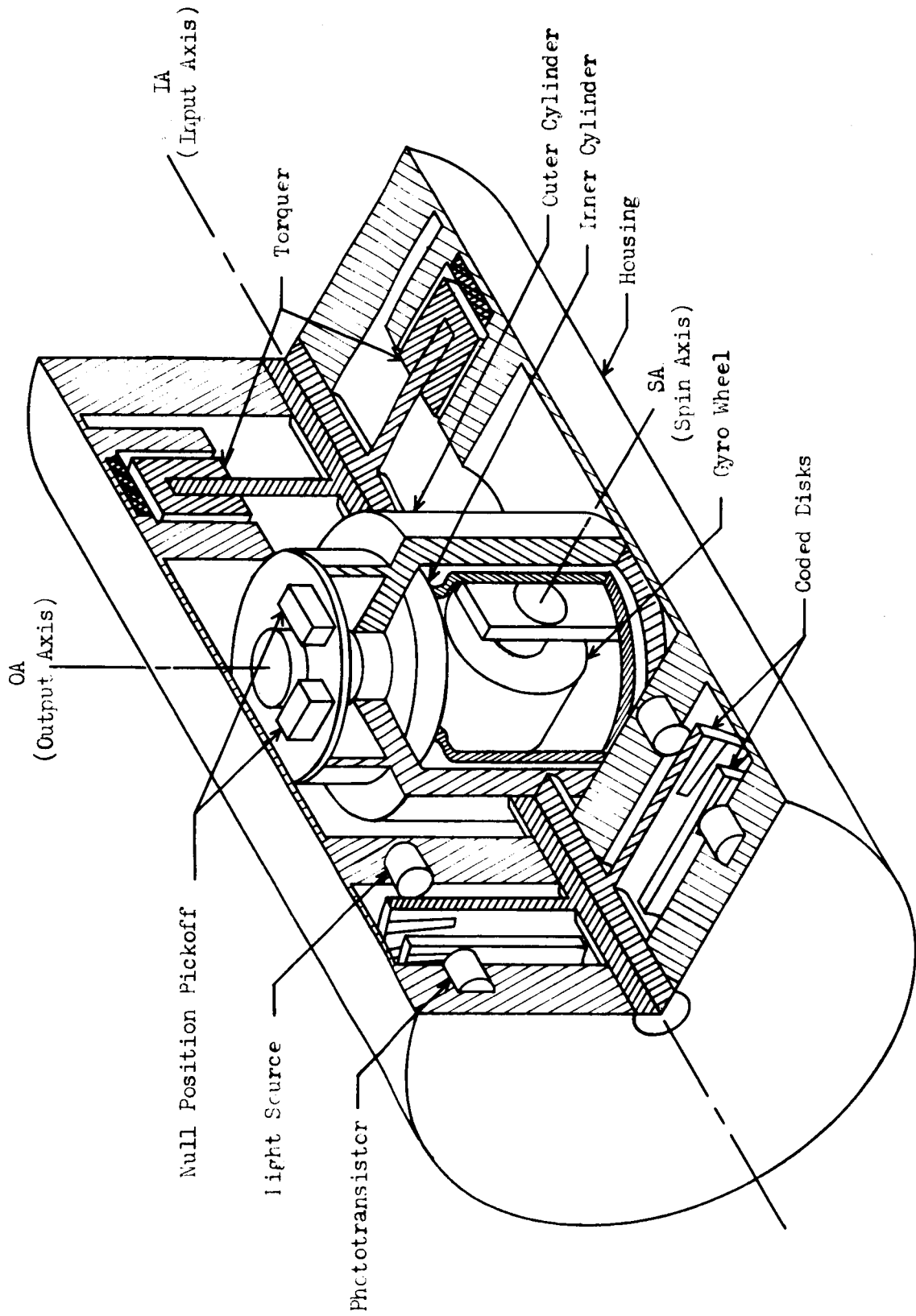


Fig. 4-- Simplified SAP

SA. In this discussion it is assumed that the case of the SAP is mounted to a heavier body whose motion will not be affected by the output of the torque motor of the SAP.

If there is an angular motion of the case about IA, the outer cylinder will remain fixed with respect to the spin axis and the case will move freely about the outer cylinder. If, due to friction or drag the outer cylinder is torqued by the movement of the case, then the gyro wheel and the inner cylinder will precess about OA. This precession will be sensed by the null position pickoff mounted at the end of the inner cylinder. The pickoff produces an electrical signal proportional to the angle sensed. This signal is fed to a servosystem whose output unit is the torquer mounted between the case and the cylinder. The torquer produces a torque on the outer cylinder about IA which will exactly oppose the original torque resulting from friction, thus compensating for friction. The movement of the case with respect to the outer cylinder will be sensed by the encoder, and the encoder will give an output signal.

If there is an angular motion of the case about OA, the outer cylinder will move with the case, while the inner cylinder will remain fixed. The angular displacement of the outer cylinder will be sensed by the null position pickoff, and an electrical signal will be generated. This signal is amplified and fed to the torquer which produces a torque on the outer cylinder about IA. This torque causes the gyro wheel and the inner cylinder to precess about OA, following the angular motion of the case. The alignment of the inner and outer cylinders with respect to the case will remain the same, and the encoder will not give an output.

If there is an angular motion of the case about SA, both the outer cylinder and the inner cylinder will move with the case. The alignments of the inner cylinder, the outer cylinder, and the case with respect to each other will remain the same, and the encoder will not give an output.

Translational motion or acceleration will not affect the output of the SAP, since it is designed with the center of mass of the gyro wheel, and the center of mass of the inner and outer cylinders, located at the intersection of IA, OA, and SA. The forces acting on the gyro wheel and outer cylinder due to translational acceleration will always produce zero torque, and therefore will not cause an angular motion of any part of the SAP.

The only motion of the SAP that will produce an output from the encoder is angular motion about IA. Thus the output of the SAP can be used to calculate the angular rate of the vehicle about the reference axis IA of the SAP. Three SAP's mounted with their reference axes aligned with the respective three axes of the vehicle's rectangular coordinate system would give the three components of the angular rate vector of the vehicle in the vehicle coordinate system.

II. DERIVATION OF THE EQUATIONS OF MOTION OF AN IDEAL SAP [1,2,4,5]

A. Introduction

A mathematical model of the ideal SAP will be developed in this chapter. The input to this mathematical model will be the angular velocity of the case of the SAP, and the output will be an angle that is the integral of the input angular velocity component along the reference axis of the SAP. A functional sketch of an ideal SAP is shown in Fig. 5, where the output angle has been designated as θ_1 . The angle θ_2 in Fig. 5 is the angle between the spin axis of the gyro wheel and a line perpendicular to the plane of the gimbal. Also shown in this sketch are three sets of rectangular coordinate axes fixed in the bodies of the float, gimbal, and case of the SAP. These three coordinate systems are randomly placed on the three bodies for ease of figure congestion, but actually they should be considered as (and will be used as) three coordinate systems with a common origin located at the intersection of the reference axis, the spin axis, and the axis of rotation of the float with respect to the gimbal. These coordinate systems will be designated by the subscripts f, g, and c for the float, gimbal, and case coordinate systems respectively; i.e., a vector \bar{F} written in the float coordinate system will be \bar{F}_f , but in the gimbal coordinate system the vector will be \bar{F}_g . Note that the three coordinate systems will align with one another when $\theta_1 = \theta_2 = 0$.

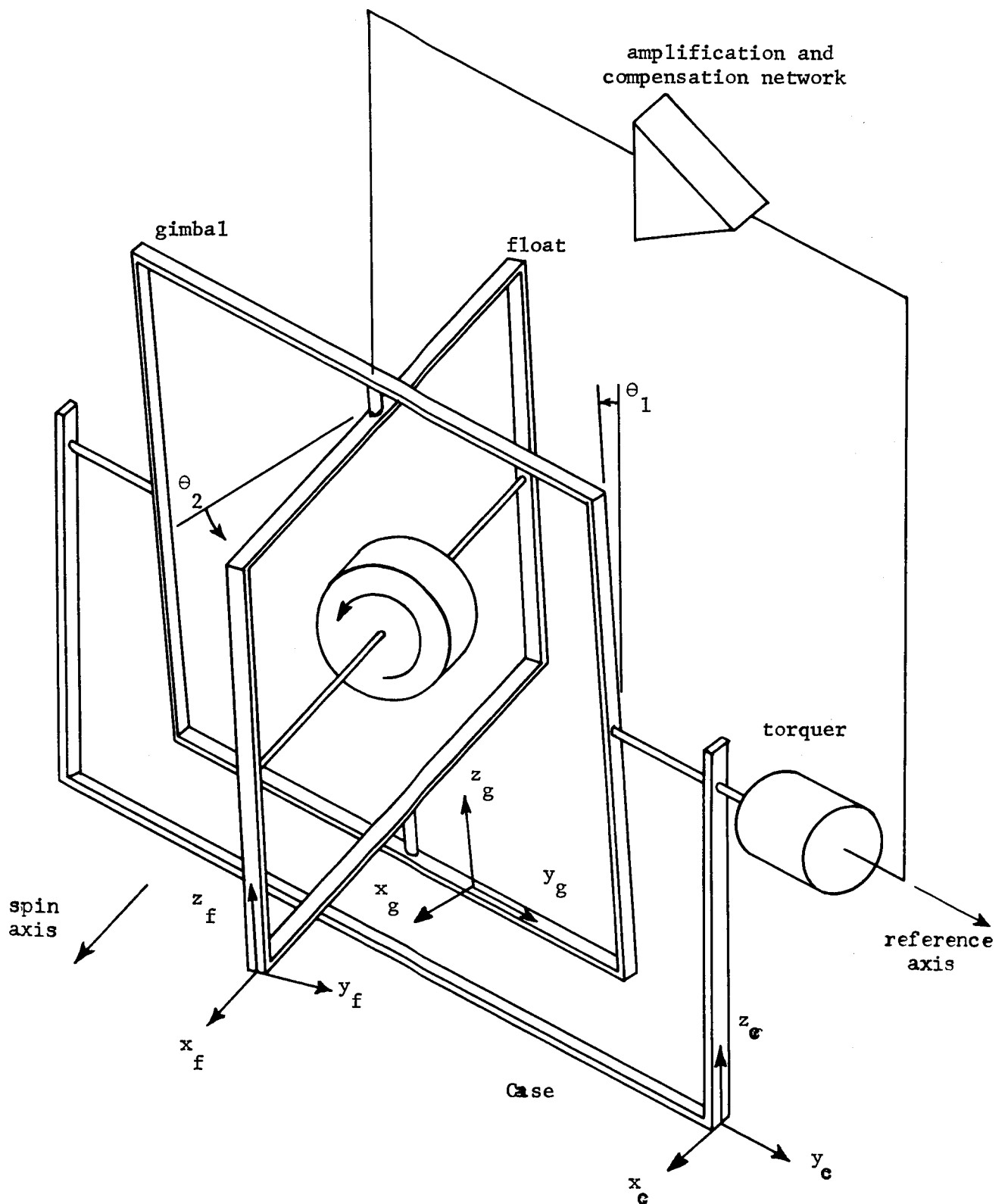


Fig. 5 --Functional sketch of an ideal SAP.

A vector written in the float coordinate system can be transformed to the gimbal coordinate system by $\bar{F}_g = C_{gf} \bar{F}_f$, where

$$C_{gf} = \begin{bmatrix} \cos\theta_2 & -\sin\theta_2 & 0 \\ \sin\theta_2 & \cos\theta_2 & 0 \\ 0 & 0 & 1 \end{bmatrix}. \quad (\text{II-1})$$

Note that when $\theta_2 = 0$, C_{gf} is the identity matrix and $\bar{F}_g = \bar{F}_f$, which means that the gimbal and float coordinate systems are aligned.

A vector written in the case coordinate system can be transformed to the gimbal coordinate system by $\bar{F}_g = C_{gc} \bar{F}_c$, where

$$C_{gc} = \begin{bmatrix} \cos\theta_1 & 0 & -\sin\theta_1 \\ 0 & 1 & 0 \\ \sin\theta_1 & 0 & \cos\theta_1 \end{bmatrix}. \quad (\text{II-2})$$

The equations governing the operation of an ideal SAP fall into two distinct classes: (1) The equations of motion of the floated gimballed gyroscope, and (2) the equations of the feedback loop, which include the compensation network, the amplifier, and the torquer. The latter division, showing the necessary inputs and outputs of the two sections, is shown in Fig. 6, where $\bar{\omega}_c$ is the angular rate vector of the case of the SAP. The output of the torquer is a torque, L_{yg} , that is applied to the gimbal of the SAP, and hence a vector along the reference axis of the SAP. This torque vector is always aligned with the y-axis of the gimbal; hence, the notation L_{yg} .

The equations of the floated gimballed gyroscope must be obtained so that they will yield the angles θ_1 and θ_2 for the inputs $\bar{\omega}_c$ and L_{yg} . The equations of the feedback loop must be obtained so that they will

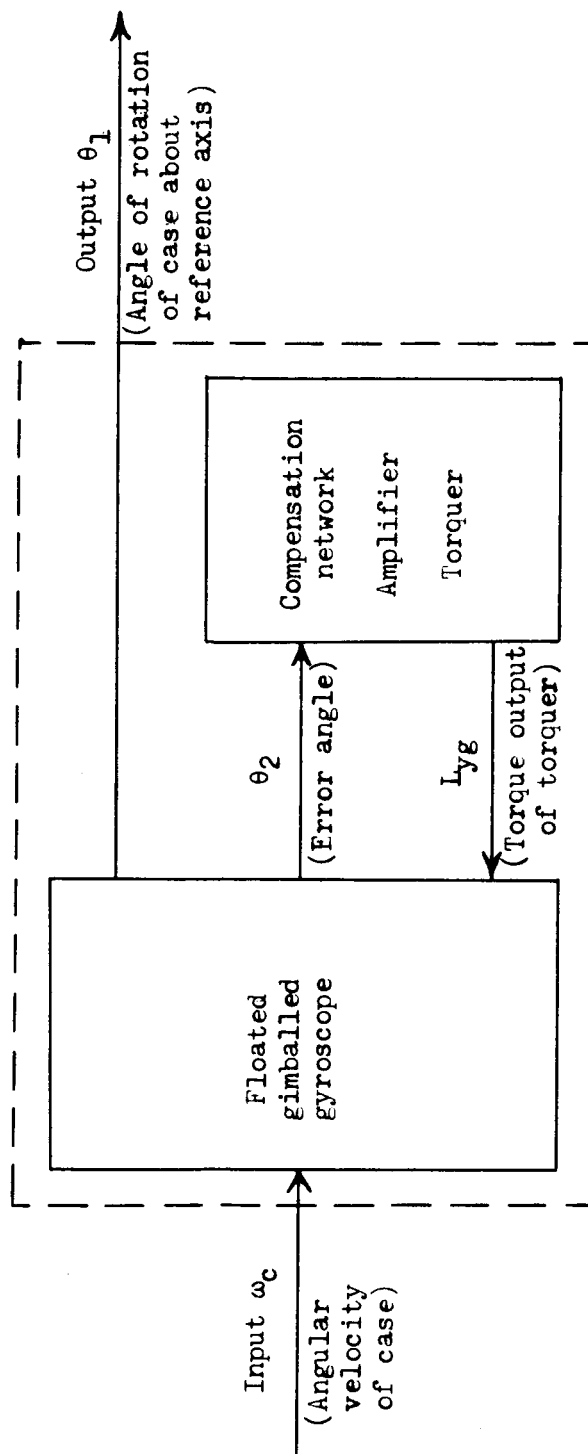


Fig. 6--Elementary block diagram of the SAP showing input-output relationships.

yield the torque L_{yg} for an input angle θ_2 . The equations of the feedback loop are assumed to be linear, thus permitting the relation between $L_{yg}(S)$ and $\theta_2(S)$ to be written as a transfer function. This transfer function was obtained from the Marshall Space Flight Center, Huntsville, Alabama, and is written

$$\frac{L_{yg}(S)}{\theta_2(S)} = K_2 H(S) = K_2 \frac{(S+100+j200)(S+100-j200)(S+50)}{(S+1)(S+6000)(S+1500+j1000)(S+1500-j1000)}, \quad (\text{II-3})$$

where K_2 is the feedback gain. Since this function is the transfer function of the feedback loop, it is called (in keeping with standard notation) $K_2 H(S)$.

The law of rotational motion, upon which the equations of this section are based, is

$$\bar{L} = \frac{d\bar{H}}{dt}, \quad (\text{II-4})$$

where \bar{L} is the externally applied torque to the rigid body, and $d\bar{H}/dt$ is the time rate of change of the angular momentum vector \bar{H} of the body. The angular momentum vector of a rigid body can be written in terms of the tensor of inertia:

$$\bar{H} = \bar{I}\bar{\omega} = \begin{bmatrix} I_{xx} & I_{xy} & I_{xz} \\ I_{yx} & I_{yy} & I_{yz} \\ I_{zx} & I_{zy} & I_{zz} \end{bmatrix} \begin{bmatrix} \omega_x \\ \omega_y \\ \omega_z \end{bmatrix}, \quad (\text{II-5})$$

where the I 's represent the moments and products of inertia, and $\bar{\omega}$ is the angular velocity of the body. If the coordinate axes are chosen fixed in the body so that they coincide with the principal axes of the body, the products of inertia are zero and the moments of inertia are constants. Under these conditions, which will hold for the set of coordinate axes used in deriving the equations of motion of the gimballed floated gyroscope, (II-5) can be written

$$\bar{H} = \begin{bmatrix} H_x \\ H_y \\ H_z \end{bmatrix} = \begin{bmatrix} I_{xx} \omega_x \\ I_{yy} \omega_y \\ I_{zz} \omega_z \end{bmatrix}, \quad (\text{II-6})$$

or

$$\bar{H} = \bar{i} I_{xx} \omega_x + \bar{j} I_{yy} \omega_y + \bar{k} I_{zz} \omega_z, \quad (\text{II-7})$$

where \bar{i} , \bar{j} and \bar{k} are unit vectors along the x , y , and z body fixed axes, respectively. The time derivative of the vector \bar{H} is

$$\begin{aligned} \frac{d\bar{H}}{dt} &= \bar{i} I_{xx} \dot{\omega}_x + \bar{j} I_{yy} \dot{\omega}_y + \bar{k} I_{zz} \dot{\omega}_z + I_{xx} \omega_x \frac{d\bar{i}}{dt} \\ &\quad + I_{yy} \omega_y \frac{d\bar{j}}{dt} + I_{zz} \omega_z \frac{d\bar{k}}{dt}, \end{aligned} \quad (\text{II-8})$$

where the dot denotes time derivative. It can be shown that (II-8) is equal to

$$\frac{d\bar{H}}{dt} = \bar{L} = \begin{bmatrix} I_{xx} \dot{\omega}_x + \omega_y \omega_z (I_{zz} - I_{yy}) \\ I_{yy} \dot{\omega}_y + \omega_x \omega_z (I_{xx} - I_{zz}) \\ I_{zz} \dot{\omega}_z + \omega_x \omega_y (I_{yy} - I_{xx}) \end{bmatrix}, \quad (\text{II-9})$$

or

$$\frac{d\bar{H}}{dt} = \bar{L} = \frac{d\bar{H}}{dt} + \bar{\omega} \times \bar{H}, \quad (\text{II-10})$$

where $\frac{d\bar{H}}{dt} = \bar{i} \dot{H}_x + \bar{j} \dot{H}_y + \bar{k} \dot{H}_z$ and $\bar{\omega} \times \bar{H}$ is the cross product.

Equation (II-9) can be written as the following three separate scalar equations:

$$\begin{aligned} I_{xx} \dot{\omega}_x + \omega_y \omega_z (I_{zz} - I_{yy}) &= L_x \\ I_{yy} \dot{\omega}_y + \omega_x \omega_z (I_{xx} - I_{zz}) &= L_y \\ I_{zz} \dot{\omega}_z + \omega_x \omega_y (I_{yy} - I_{xx}) &= L_z, \end{aligned} \quad (\text{II-11})$$

where L_x , L_y and L_z are the components of the externally applied torque along the x, y, and z axes of the body fixed coordinate system, respectively. The three scalar equations in (II-11) are Euler's equations referred to the principal axes of the body.

B. Derivation of the Float Torque Equation

The angular momentum vector of the gyro wheel, written in the float coordinate system, is

$$\bar{H}_{wf} = \begin{bmatrix} I_{xxw} (\omega_{xf} + \omega_s) \\ I_{yyw} (\omega_{yf}) \\ I_{zzw} (\omega_{zf}) \end{bmatrix}, \quad (\text{II-12})$$

where I_{xxw} , I_{yyw} and I_{zzw} are the moments of inertia of the gyro wheel about the float coordinate axis, ω_s is the assumed constant angular velocity of the wheel measured with respect to the float, and ω_{xf} , ω_{yf} and ω_{zf} are the components of the angular velocity of the float written in the float coordinate system.

The angular momentum vector of the float, not including the gyro wheel, written in the float coordinate system is

$$\bar{H}_{ff} = \begin{bmatrix} I_{xxf} \omega_{xf} \\ I_{yyf} \omega_{yf} \\ I_{zzf} \omega_{zf} \end{bmatrix}, \quad (\text{II-13})$$

where I_{xxf} , I_{yyf} and I_{zzf} are the moments of inertia of the float about the float coordinate axes, and ω_{xf} , ω_{yf} and ω_{zf} are the components of the angular velocity of the float written in the float coordinate system.

The angular momentum vector of the float-wheel combination, written in the float coordinate system, is

$$\bar{H}_{(fw)f} = \bar{H}_{ff} + \bar{H}_{wf} = \begin{bmatrix} I_{xf}\omega_{xf} + H_w \\ I_{yf}\omega_{yf} \\ I_{zf}\omega_{zf} \end{bmatrix}, \quad (\text{II-14})$$

where

$$\begin{aligned} I_{xf} &= I_{xxw} + I_{xxf}, \\ I_{yf} &= I_{yyw} + I_{yyf}, \\ I_{zf} &= I_{zzw} + I_{zzf}, \end{aligned}$$

and H_w is the magnitude of the component of the angular momentum of the gyro wheel resulting from the angular velocity ω_s , i.e., $H_w = I_{xxw}\omega_s$.

The float torque equations can be obtained from (II-14) by performing the operations indicated in (II-9) or (II-10). The resulting equation is

$$\bar{L}_f = \begin{bmatrix} \dot{\omega}_{xf} I_{xf} + \omega_{yf} \omega_{zf} (I_{zf} - I_{yf}) \\ \dot{\omega}_{yf} I_{yf} + \omega_{xf} \omega_{zf} (I_{xf} - I_{zf}) + \omega_{zf} H_w \\ \dot{\omega}_{zf} I_{zf} + \omega_{xf} \omega_{yf} (I_{yf} - I_{xf}) - \omega_{yf} H_w \end{bmatrix}. \quad (\text{II-15})$$

Equation (II-15) represents Euler's equations modified to include the momentum of the gyro wheel rotating at an assumed constant velocity ω_s .

C. Derivation of the Gimbal Torque Equation

The gimbal torque equation can be developed by means of a similar procedure to that used to develop the float torque equation.

The angular momentum vector of the gimbal (not including the float-wheel combination), written in the gimbal coordinate system is

$$\bar{H}_{gg} = \begin{bmatrix} I_{xg} \omega_{xg} \\ I_{yg} \omega_{yg} \\ I_{zg} \omega_{zg} \end{bmatrix}, \quad (\text{II-16})$$

where I_{xg} , I_{yg} and I_{zg} are the moments of inertia of the gimbal about the gimbal coordinate axes, and ω_{xg} , ω_{yg} , and ω_{zg} are the components of the angular velocity of the gimbal written in the gimbal coordinate system.

The angular momentum vector of the float-wheel combination written in the gimbal coordinate system can be obtained from the $\bar{H}_{(fw)f}$ in (II-14) by using the transformation in (II-1); i.e., $\bar{H}_{(fw)g} = C_{gf} \bar{H}_{(fw)f}$, or

$$\bar{H}_{(fw)g} = \begin{bmatrix} \cos \theta_2 & -\sin \theta_2 & 0 \\ \sin \theta_2 & \cos \theta_2 & 0 \\ 0 & 0 & 1 \end{bmatrix} \begin{bmatrix} I_{xf} \omega_{xf} + H_w \\ I_{yf} \omega_{yf} \\ I_{zf} \omega_{zf} \end{bmatrix}. \quad (\text{II-17})$$

The angular momentum vector of the gimbal-float-wheel combination, written in the gimbal coordinate system, is

$$\bar{H}_{(gfw)g} = \begin{bmatrix} I_{xg} \omega_{xg} \\ I_{yg} \omega_{yg} \\ I_{zg} \omega_{zg} \end{bmatrix} + \begin{bmatrix} \cos \theta_2 & -\sin \theta_2 & 0 \\ \sin \theta_2 & \cos \theta_2 & 0 \\ 0 & 0 & 1 \end{bmatrix} \begin{bmatrix} I_{xf} \omega_{xf} + H_w \\ I_{yf} \omega_{yf} \\ I_{zf} \omega_{zf} \end{bmatrix},$$

(II-18)

or

$$\bar{H}_{(gfw)g} = \begin{bmatrix} I_{xg} \omega_{xg} + H_w \cos \theta_2 + I_{xf} \omega_{xf} \cos \theta_2 \\ -I_{yf} \omega_{yf} \sin \theta_2 \\ I_{yg} \omega_{yg} + H_w \sin \theta_2 + I_{xf} \omega_{xf} \sin \theta_2 \\ +I_{yf} \omega_{yf} \cos \theta_2 \\ I_{zg} \omega_{zg} + I_{zf} \omega_{zf} \end{bmatrix}. \quad (II-19)$$

The gimbal torque equation can be obtained from (II-19) by performing the operations indicated in (II-9) or (II-10). The resulting equation is

$$\begin{aligned}
& \omega_{yg} \omega_{zg} (I_{zg} - I_{yg}) + \omega_{yg} \omega_{zf} I_{zf} \\
& -H_w \sin \theta_2 (\omega_{zg} + \dot{\theta}_2) - \omega_{zg} \omega_{xf} I_{xf} \sin \theta_2 \\
& -\omega_{zg} \omega_{yf} I_{yf} \cos \theta_2 + \dot{\omega}_{xg} I_{xg} + \dot{\omega}_{xf} I_{xf} \cos \theta_2 \\
& -\omega_{xf} \dot{\theta}_2 I_{xf} \sin \theta_2 - \dot{\omega}_{yf} I_{yf} \sin \theta_2 \\
& \quad -\omega_{yf} \dot{\theta}_2 I_{yf} \cos \theta_2 \\
& \omega_{zg} \omega_{xg} (I_{xg} - I_{zg}) + \omega_{zg} H_w \cos \theta_2 \\
& +\omega_{zg} \omega_{xf} I_{xf} \cos \theta_2 - \omega_{zg} \omega_{yf} I_{yf} \sin \theta_2 \\
\bar{L}_g = & -\omega_{xg} \omega_{zf} I_{zf} + \dot{\omega}_{yg} I_{yg} + \dot{\theta}_2 (H_w \cos \theta_2 \\
& +\omega_{xf} I_{xf} \cos \theta_2 - \omega_{yf} I_{yf} \sin \theta_2) \\
& +\omega_{xf} I_{xf} \sin \theta_2 + \dot{\omega}_{yf} I_{yf} \cos \theta_2 \\
& \omega_{xg} \omega_{yg} (I_{yg} - I_{xg}) + \omega_{xg} H_w \sin \theta_2 \\
& +\omega_{xg} \omega_{xf} I_{xf} \sin \theta_2 + \omega_{xg} \omega_{yf} I_{yf} \cos \theta_2 \\
& -\omega_{yg} H_w \cos \theta_2 - \omega_{yg} \omega_{xf} I_{xf} \cos \theta_2 \\
& +\omega_{yg} \omega_{yf} I_{yf} \sin \theta_2 + \dot{\omega}_{zg} I_{zg} \\
& \quad + \dot{\omega}_{zf} I_{zf}
\end{aligned}
\tag{II-20}$$

D. Derivation of the Block Diagram
of an Ideal SAP

The float of an ideal SAP is mounted to the gimbal so that the torque transferred from the gimbal to the float through the mount cannot have a component along the z-axis of the float. Therefore, in an ideal SAP L_{zf} is zero. L_{zf} will not be set equal to zero in the following work, because its inclusion in the equations to be developed will permit them to be used to represent the equations of motion of a Pendulous Integrating Gyro Accelerometer (PIGA). L_{zf} can also be considered as a possible error torque. From (II-15),

$$L_{zf} = \dot{\omega}_{zf} I_{zf} + \omega_{xf} \omega_{yf} (I_{yf} - I_{xf}) - \omega_{yf} H_w . \quad (\text{II-21})$$

The gimbal of an ideal SAP is mounted to the case so that the torque transferred through the mount is zero along the y-axis of the gimbal. The output of the torque motor that is mounted between the gimbal and the case is a torque on the gimbal that is always along the y-axis of the gimbal. Therefore, the component of the external torque applied to the gimbal-float-wheel combination of an ideal SAP along the y-axis of the gimbal is the output of the torque motor. In the following work it will be assumed that L_{yg} can contain a component of error torque, L_{yge} , resulting from friction or drag.

From (II-20),

$$\begin{aligned}
 L_{yg} = & \omega_{zg} \omega_{xg} (I_{xg} - I_{zg}) + \omega_{zg} H_w \cos \theta_2 \\
 & + \omega_{zg} \omega_{xf} I_{xf} \cos \theta_2 - \omega_{zg} \omega_{yf} I_{yf} \sin \theta_2 \\
 & - \omega_{xg} \omega_{zf} I_{zf} + \omega_{yg} \dot{I}_{yg} + \dot{\theta}_2 (H_w \cos \theta_2 \\
 & + \omega_{xf} I_{xf} \cos \theta_2 - \omega_{yf} I_{yf} \sin \theta_2) \\
 & + \omega_{xf} \dot{I}_{xf} \sin \theta_2 + \dot{\omega}_{yf} I_{yf} \cos \theta_2 .
 \end{aligned} \tag{II-22}$$

It can be seen from the functional sketch of Fig. 5, under the condition $\theta_2 \approx 0$, that

$$\begin{aligned}
 \omega_{zf} - \omega_{zg} &= \dot{\theta}_2 , \\
 \omega_{xf} &\approx \omega_{xg} , \\
 \omega_{yf} &\approx \omega_{yg} ,
 \end{aligned} \tag{II-23}$$

and

$$\dot{\omega}_{yf} \approx \dot{\omega}_{yg} .$$

Using the relations in (II-23), together with $\cos \theta_2 \approx 1$ and $\sin \theta_2 \approx 0$, in (II-21) and (II-22), gives

$$\dot{L}_{zf} = \dot{\omega}_{zf} I_{zf} + \omega_{xf} \omega_{yf} (I_{yf} - I_{xf}) - \omega_{yg} H_w, \quad (\text{II-24})$$

and

$$\begin{aligned} L_{yg} = & \omega_{zg} \omega_{xg} (I_{xg} + I_{xf} - I_{zg} - I_{zf}) \\ & + H_w (\omega_{zg} + \dot{\theta}_2) + \omega_{xg} \dot{\theta}_2 (I_{xf} - I_{zf}) \\ & + \dot{\omega}_{yg} (I_{yg} + I_{yf}). \end{aligned} \quad (\text{II-25})$$

Since the angular momentum of the gyro wheel is large (ω_s large),

$$\begin{aligned} |\omega_{xg} (I_{xg} + I_{xf} - I_{zg} - I_{zf})| &<< H_w, \\ |\omega_{xf} (I_{yf} - I_{xf})| &<< H_w, \end{aligned} \quad (\text{II-26})$$

and

$$|\omega_{xg} (I_{xf} - I_{zf})| << H_w.$$

Using (II-26) in (II-24) and (II-25), and rearranging terms, gives

$$\dot{\omega}_{zf} = \frac{1}{I_{zf}} (\dot{L}_{zf} + \omega_{yg} H_w), \quad (\text{II-27})$$

and

$$\dot{\omega}_{yg} = \frac{1}{I_{yg} + I_{yf}} (L_{yg} - \omega_{zf} H_w) . \quad (\text{II-28})$$

Inspection of Fig. 5 yields the following equations:

$$\dot{\theta}_1 = \omega_{yg} - \omega_{yc} , \quad (\text{II-29})$$

and

$$\omega_{zg} = \omega_{xc} \sin \theta_1 + \omega_{zc} \cos \theta_1 . \quad (\text{II-30})$$

A signal flow graph of the floated gimbaled gyroscope can be constructed from (II-27), (II-28), (II-29) and (II-30), and is shown in Fig. 7.

The addition of the feedback loop to the signal flow graph of Fig. 7 gives the signal flow graph of an ideal SAP in Fig 8. A block diagram of an ideal SAP is shown in Fig. 9.

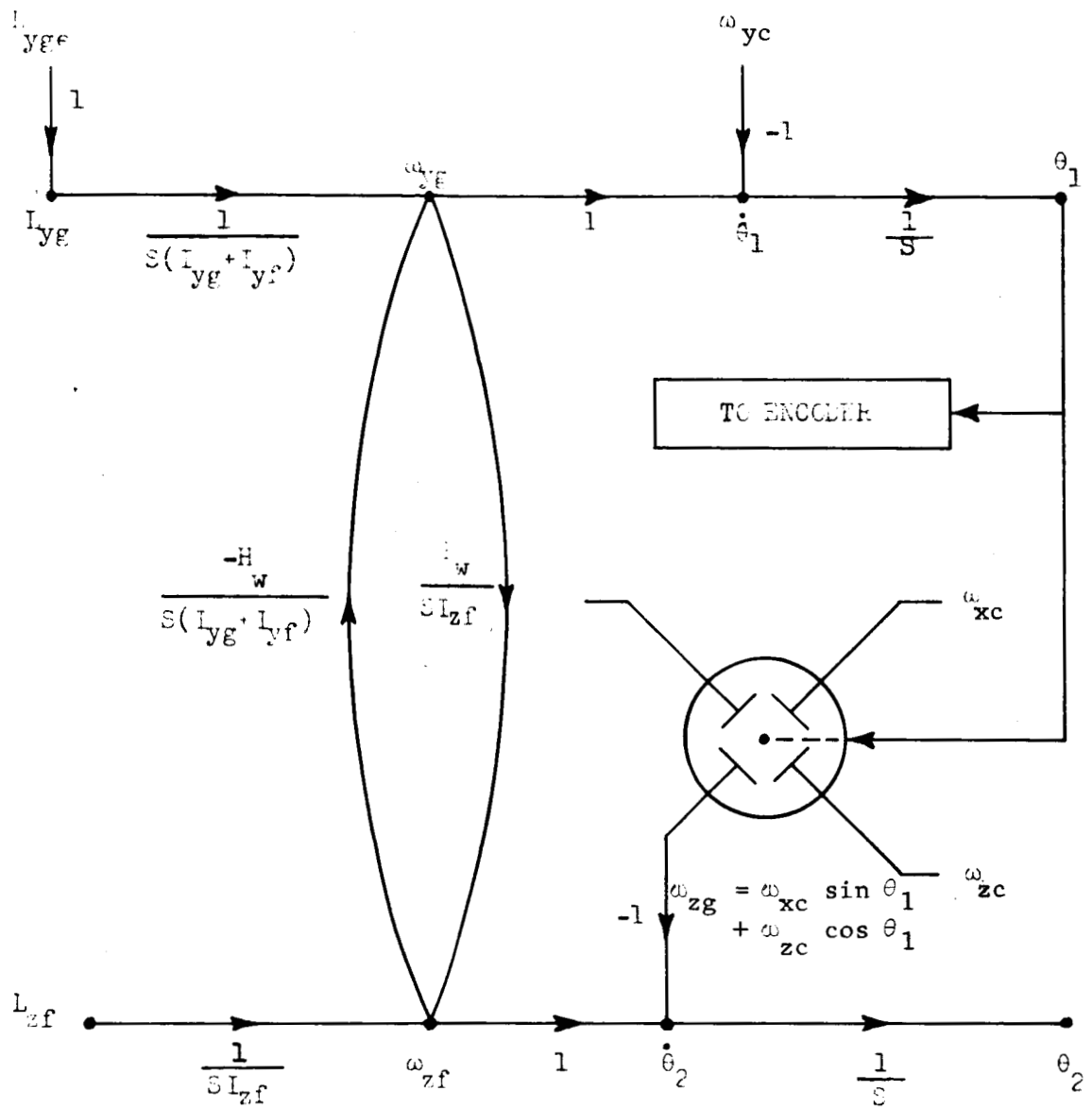


Fig. 7--Signal flow graph of an ideal floated gimbaled gyroscope.

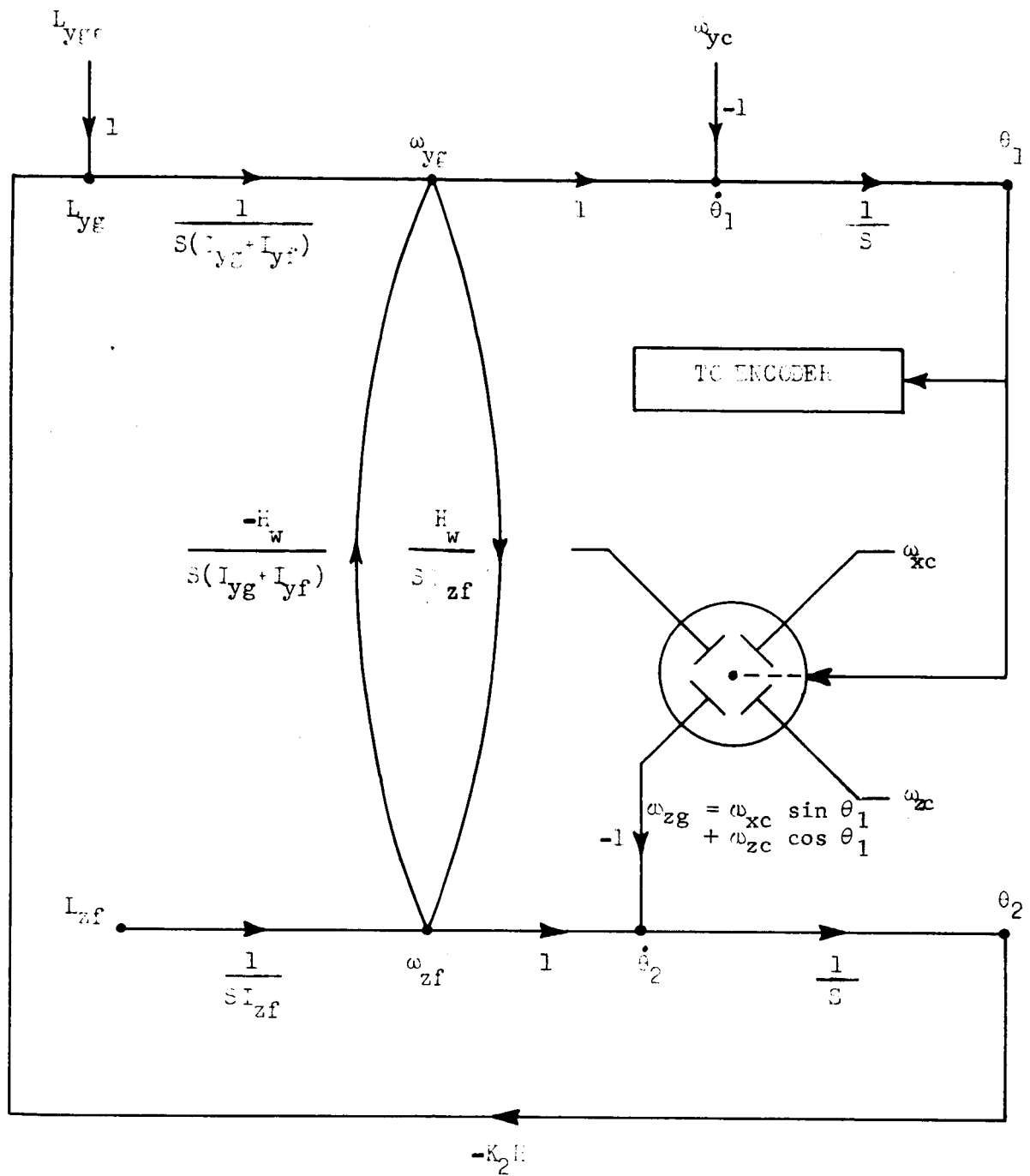


Fig. 8--Signal flow graph of an ideal SAP.

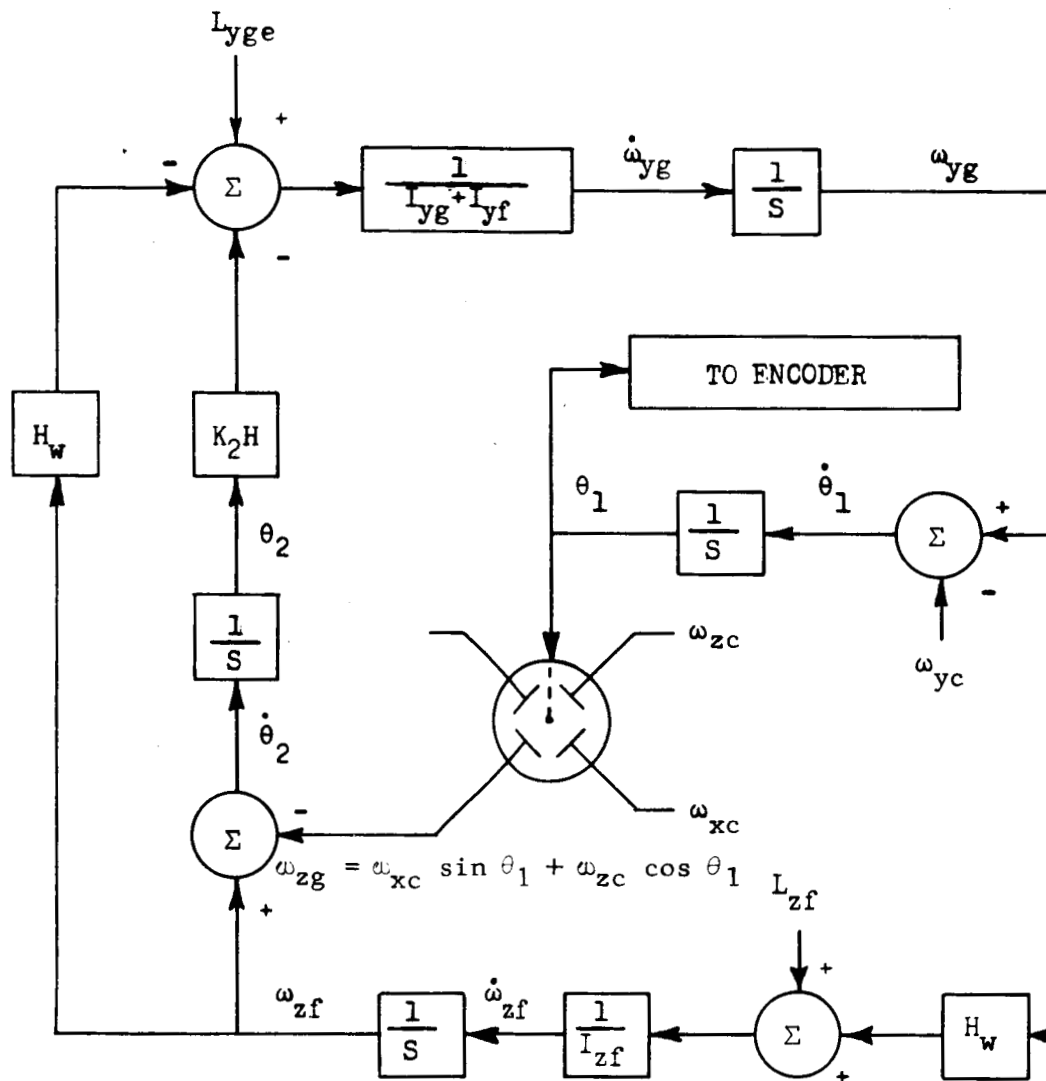


Fig. 9--Block diagram of an ideal SAP.

III. DERIVATION OF THE EQUATIONS OF MOTION OF AN IDEAL SAP WHEN THE TORSIONAL STIFFNESS OF THE GAS BEARING BETWEEN THE GIMBAL AND FLOAT IS CONSIDERED [1,6,7]

The gas suspension bearing between the gimbal and float of an ideal SAP was considered in Chapter II as a perfect frictionless bearing with perfect coupling between the gimbal and the float. A better representation of the gas bearing is obtained by assuming that the motion of the gimbal about its y-axis is coupled to the float through a shaft with finite torsional stiffness, instead of through a rigid shaft. Fig. 10 is a functional sketch of the SAP, where the finite torsional stiffness of the gas bearing has been incorporated by separating the gimbal into two gimbals coupled together by a shaft having a torsional stiffness constant, K_b . The inner gimbal has been added for mathematical convenience, and it will be considered massless since it does not exist in the physical SAP. The torsional stiffness constant, K_b , will be a function of the gas pressure; hence, as the gas pressure decreases, K_b decreases.

The equations of motion of an ideal SAP, when the torsional stiffness of the gas bearing is considered finite, can be derived in a manner similar to that used in Chapter II.

The addition of finite torsional stiffness does not change the derivation of the float torque equation except that $\omega_{yf} \approx \omega_{ygi}$ instead of $\omega_{yf} \approx \omega_{yg}$. Therefore, the float torque equation is the same as (II-27) except that ω_{yg} is replaced by ω_{ygi} :

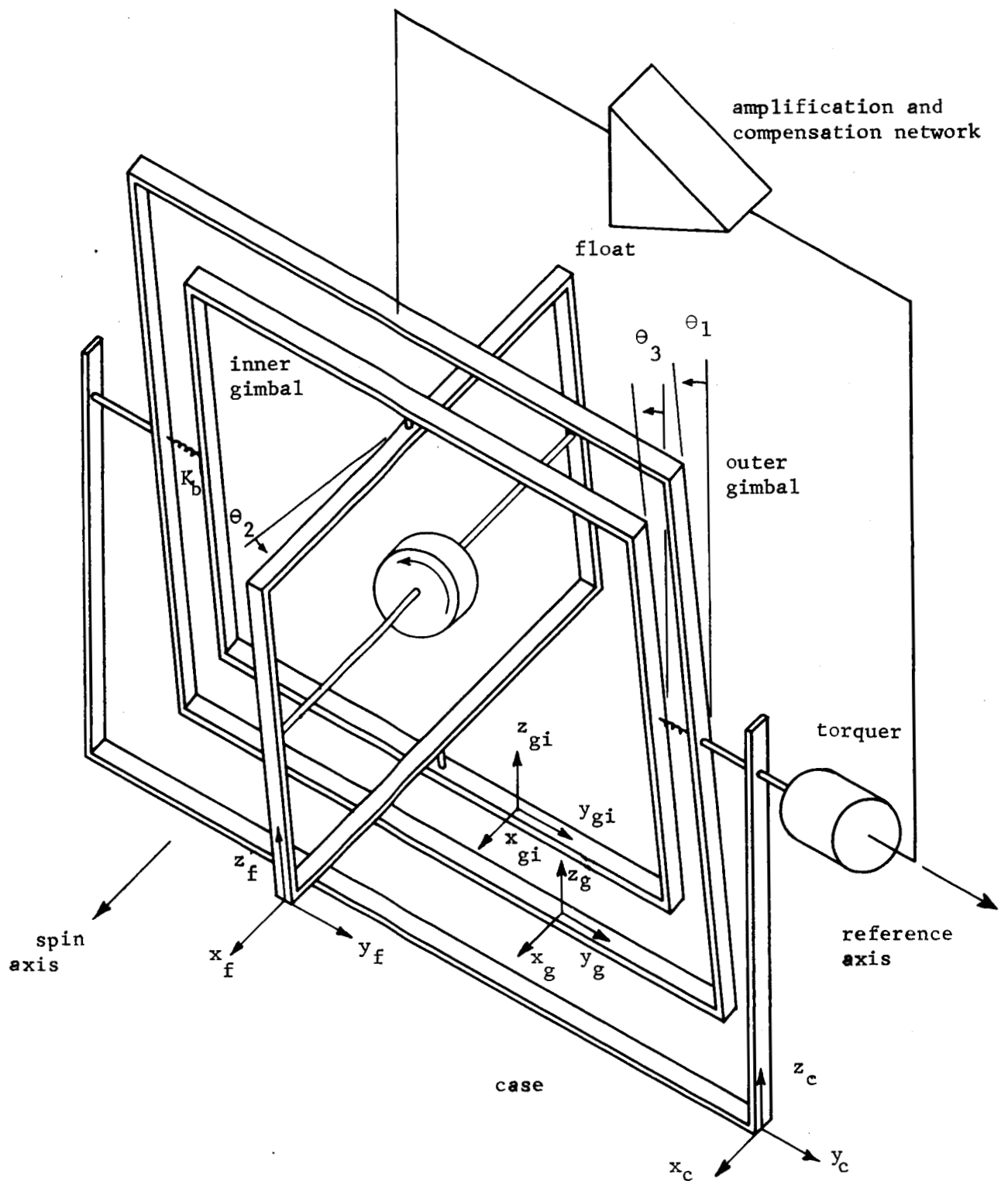


Fig. 10--Functional sketch of an ideal SAP with a finite torsional stiffness gas bearing.

$$\dot{\omega}_{zf} = \frac{1}{I_{zf}} (L_{zf} + \omega_{ygi} H_w) . \quad (\text{III-1})$$

The gimbal torque equation for infinite torsional stiffness, (II-28), can be modified to give the inner gimbal torque equation for the SAP when finite torsional stiffness is considered. This modification can be accomplished by realizing that the torque transmitted through the torsional shaft to the inner gimbal is $K_b(\theta_1 - \theta_3)$, and that the mass of the inner gimbal is zero. Incorporating these two facts into (II-28) gives the inner gimbal torque equation,

$$\dot{\omega}_{ygi} = \frac{1}{I_{yf}} [(\theta_1 - \theta_3) K_b - \omega_{zf} H_w] . \quad (\text{III-2})$$

The outer gimbal torque equation can be derived by performing the operations in (II-9) or (II-10) on the \bar{H}_g given in (II-16); i.e.,

$$\bar{L}_g = \frac{d\bar{H}_{gg}}{dt} ,$$

where \bar{L}_g is the externally applied torque to the outer gimbal, and \bar{H}_{gg} is the angular momentum vector of the gimbal. The externally applied torque along the y-axis of the gimbal is the output torque of the motor, plus the error torque L_{yge} , minus the torque $K_b(\theta_1 - \theta_3)$. The outer gimbal torque equation is

$$\dot{\omega}_{yg} = \frac{1}{I_{yg}} [L_{yg} - (\theta_1 - \theta_3) K_b - \omega_{zg} \omega_{xg} (I_{xg} - I_{zg})] , \quad (\text{III-3})$$

where L_{yg} is the sum of the output torque of the torquer and the error torque, and I_{yg} is the sum of the moments of inertia of the gimbal, the torquer rotor, and the shaft about the y-axis of the gimbal. Since $|\omega_{xg} (I_{xg} - I_{zg})| < |H_w|$, (III-3) can be written

$$\dot{\theta}_{yg} = \frac{1}{I_{yg}} [L_{yg} - (\theta_1 - \theta_3) K_b] \quad (III-4)$$

It can be seen from the functional sketch of Fig. 10 (under the conditions that $\theta_2 \approx 0$, and that $\theta_1 - \theta_3$ is small), that

$$\begin{aligned} \dot{\theta}_1 &= \omega_{yg} - \omega_{yc} , \\ \dot{\theta}_2 &= \omega_{zf} - \omega_{zgi} , \\ \dot{\theta}_1 - \dot{\theta}_3 &= \omega_{yg} - \omega_{ygi} , \\ \omega_{zgi} &\approx \omega_{zg} , \\ \omega_{ygi} &\approx \omega_{yf} , \end{aligned} \quad (III-5)$$

and

$$\dot{\omega}_{ygi} \approx \dot{\omega}_{yf} .$$

A signal flow graph of an ideal floated gimballed gyroscope with finite torsional stiffness of the gas bearing can be constructed from (III-1), (III-2), (III-4), and (III-5), and is shown in Fig. 11. The incorporation of the feedback loop in the signal flow graph of Fig. 11

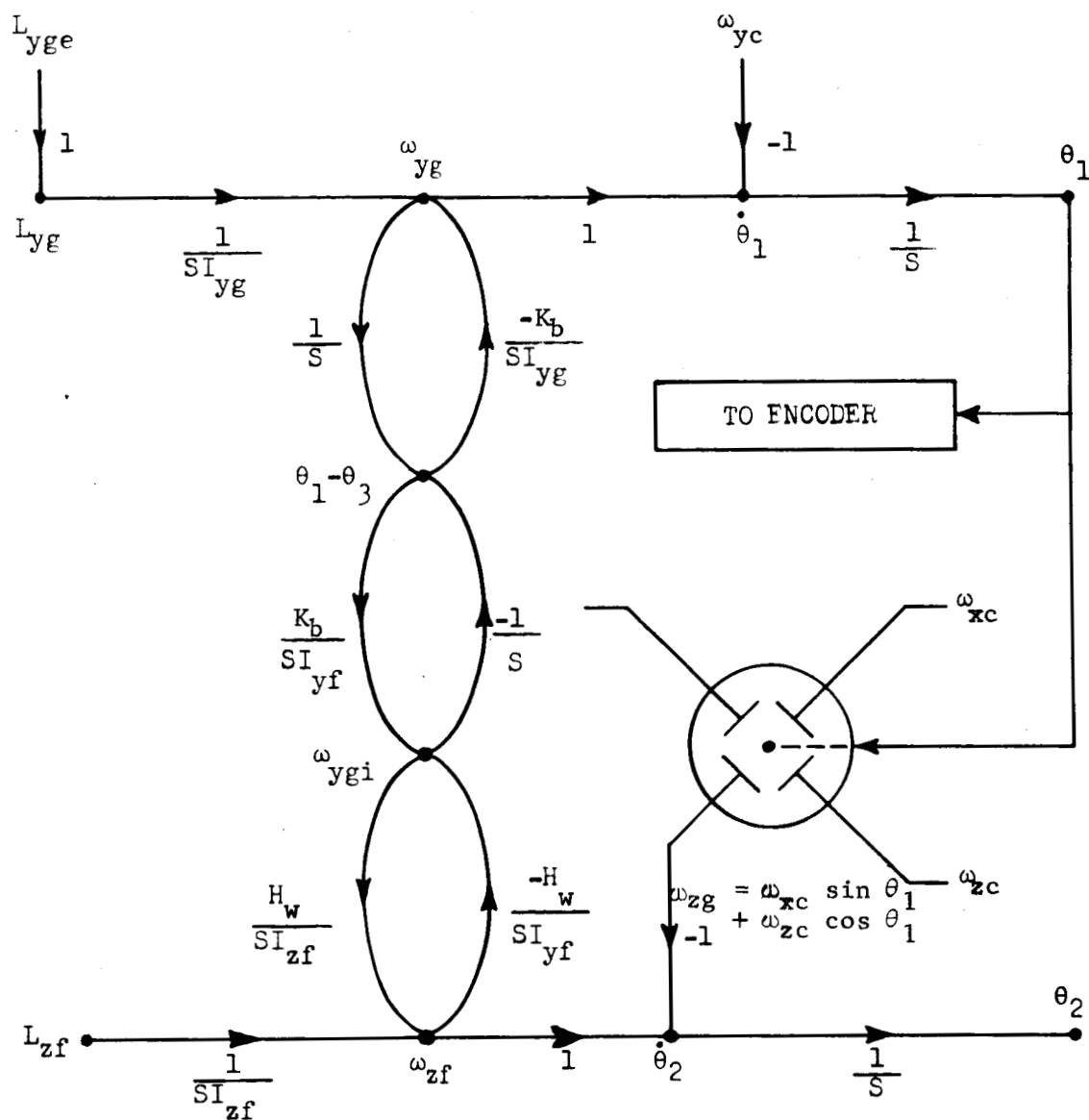


Fig. 11--Signal flow graph of an ideal floated gimballed gyroscope with a finite torsional stiffness gas bearing.

yields the signal flow graph of the ideal SAP with finite torsional stiffness of the gas bearing shown in Fig. 12. A block diagram of an ideal SAP with finite torsional stiffness of the gas bearing is shown in Fig. 13.

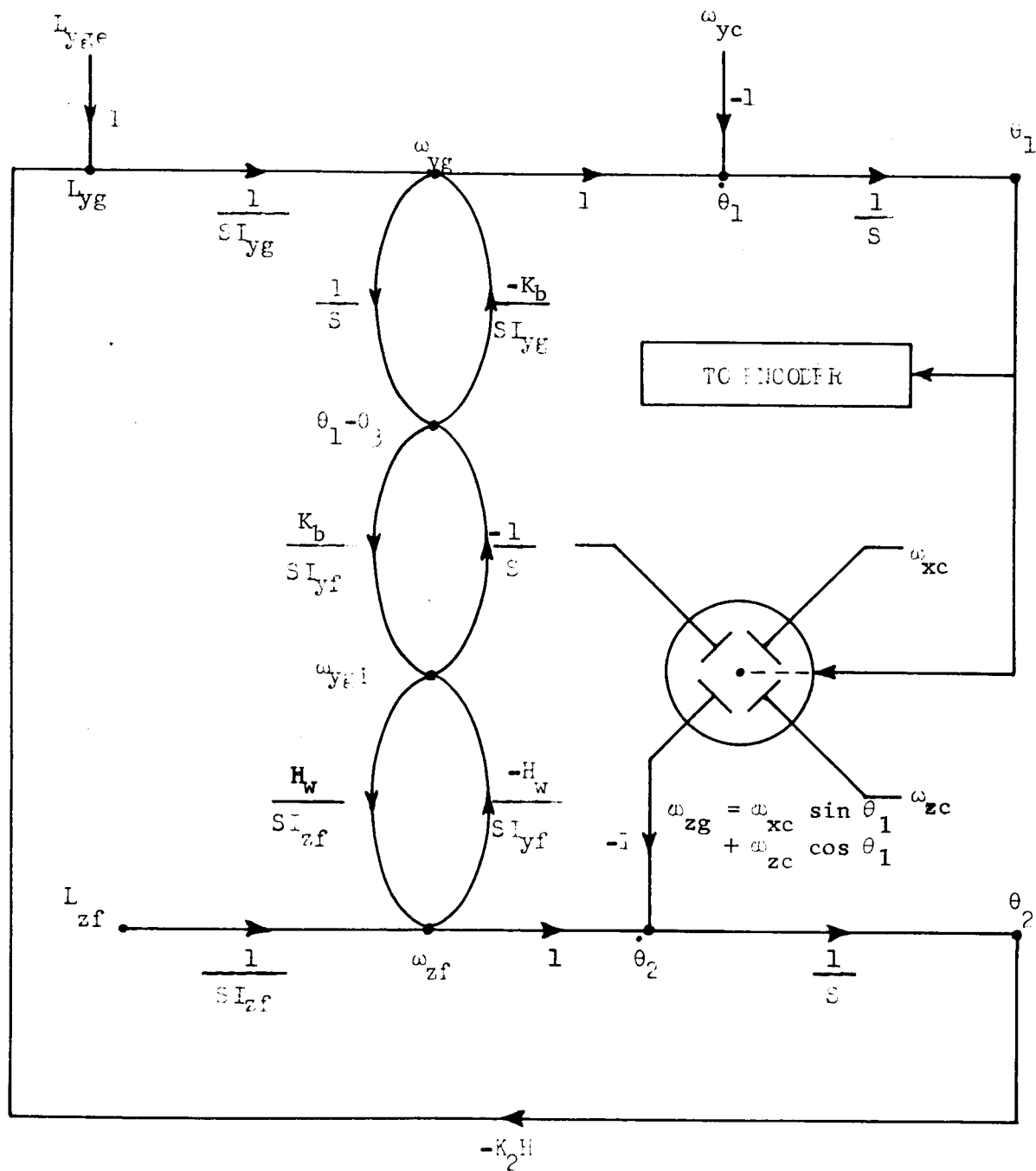


Fig. 12--Signal flow graph of an ideal SAP with a finite torsional stiffness gas bearing.

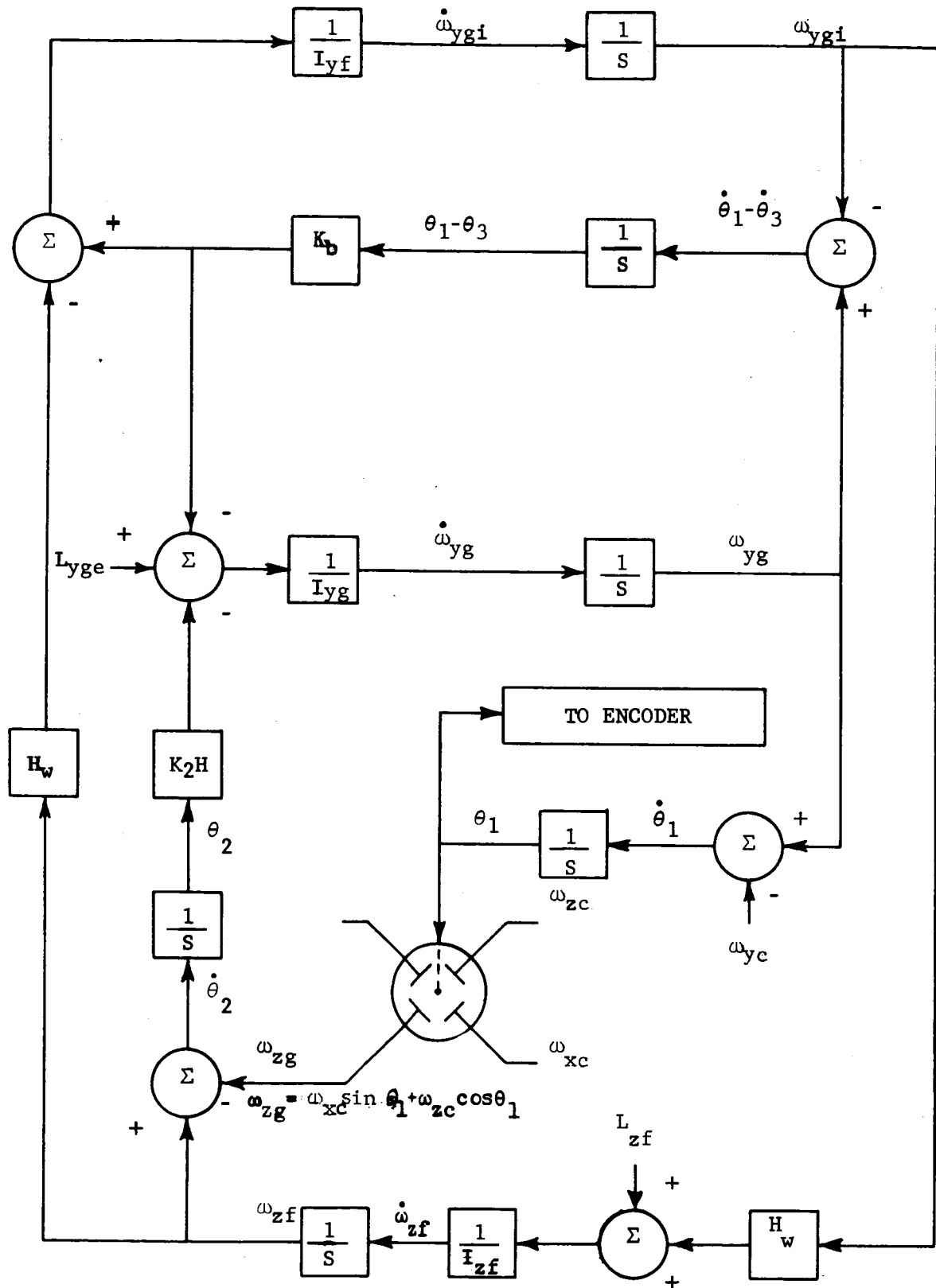


Fig. 13--Block diagram of an ideal SAP with a finite torsional stiffness gas bearing.

IV. STABILITY ANALYSIS[8,9]

A. Introduction

The stability of the floated gimballed gyroscope working in conjunction with the feedback loop is of prime importance in the operation of ideal SAP. This stability can be studied by assuming that the input angular velocity of the case is zero and treating the floated gimballed gyroscope and the feedback loop as a conventional feedback system. Under the condition of zero angular velocity of the case, the block diagram of the SAP in Fig. 9 can be simplified to give the block diagram in Fig. 14. In Fig. 14 the error torque about the Y- axis of the gimbal, L_{yge} , is considered as the input, and the error angle, θ_2 , is considered as the output. Even though the value of $\theta_2(t)$ for a given input error torque $L_{yge}(t)$ is not the desired output-input relation for the operation of an ideal SAP, its investigation will give very useful information about the stability of the SAP. The transfer function of Fig. 14. is

$$\frac{\theta_2(s)}{L_{yge}(s)} = \frac{K_1 G(s)}{1 + K_1 K_2 H(s) G(s)}, \quad (IV-1)$$

where $K_1 G(s)$ is the transfer function of the floated gimballed gyroscope, and $K_2 H(s)$ is the transfer function of the feedback path. $K_2 H(s)$ is given in (II-3) and is repeated here for convenience;

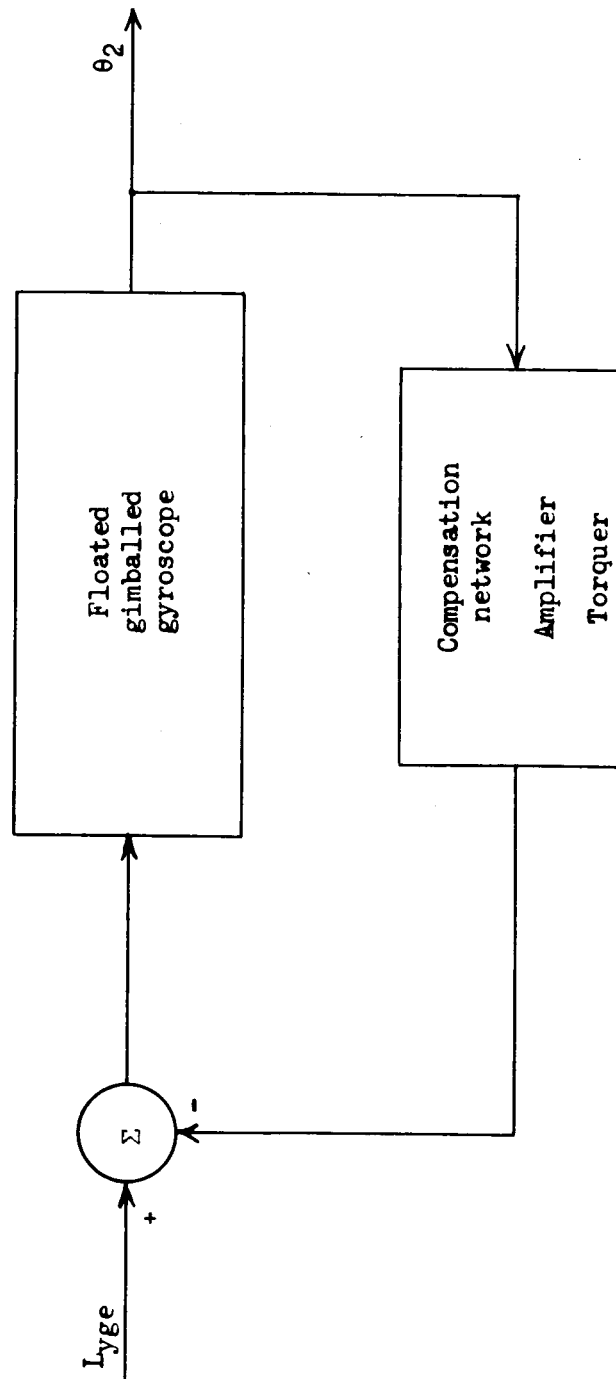


Fig. 14--Simplified block diagram of the SAP for stability analysis.

$$K_2 H(S) = \frac{K_2 (S + 100 + j200)(S + 100 - j200)(S + 50)}{(S + 1)(S + 6000)(S + 1500 + j1000)(S + 1500 - j1000)} \quad (IV-2)$$

B. Stability of an Ideal SAP
With Infinite Torsional Stiffness of the Gas Bearing

Analysis of the signal flow graph of the floated gimballed gyroscope in Fig. 7 yields the following transfer function, relating the Laplace Transform of the error angle θ_2 to the Laplace Transform of the applied torque L_{yg} :

$$K_1 G(S) = \frac{\theta_2(S)}{L_{yg}(S)} = \frac{\frac{H_W}{I_{zf}(I_{yg} + I_{yf})}}{s(s^2 + \frac{H_W}{I_{zf}(I_{yg} + I_{yf})})} \quad (IV-3)$$

Equation (IV-3) is restricted in its use, since in the derivation of the signal flow graph in Fig. 7, $\theta_2(t)$ was assumed to be very small so that $\cos \theta_2 \approx 1$ and $\sin \theta_2 \approx 0$. An analysis of (IV-3) indicates that the operation of the floated gimballed gyroscope under the limitations of very small θ_2 is oscillatory with poles on the imaginary axis at $S = 0, \pm j \frac{H_W}{\sqrt{I_{zf}(I_{yg} + I_{yf})}}$.

In order to comprehend more fully the requirements for stability of an ideal SAP, a typical set of numerical values will be used. These numerical values, which were obtained from information

furnished by Marshall Space Flight Center in Huntsville, Alabama,
are

$$H_W = 2.51 \times 10^6 \text{ gm cm}^2/\text{sec} , \quad (\text{IV-4})$$

$$I_{zf} = 2.0 \times 10^3 \text{ gm cm}^2 ,$$

and

$$I_{yg} + I_{yf} = 2.0 \times 10^4 \text{ gm cm}^2 .$$

Substituting the values of (IV-4) into (IV-3) gives the transfer function of the floated gimbaled gyroscope:

$$K_1 G(S) = \frac{6.28 \times 10^{-2}}{S(S^2 + (400)^2)} . \quad (\text{IV-5})$$

The root locus plot of the characteristic equation of (IV-1), with $K_1 G(S)$ from (IV-5) and $K_2 H(S)$ from (IV-2), for variations of the gain $K = K_1 K_2$, is shown in Fig. 15.

In Fig. 15 the loci cross the $j\omega$ axis at $\pm j 1355$ for $K = 40 \times 10^{12}$. Therefore, the ideal SAP is stable for all $K < 40 \times 10^{12}$. An operating gain of 10.0×10^{12} will furnish good stability with the closed-loop poles located in the S-plane at

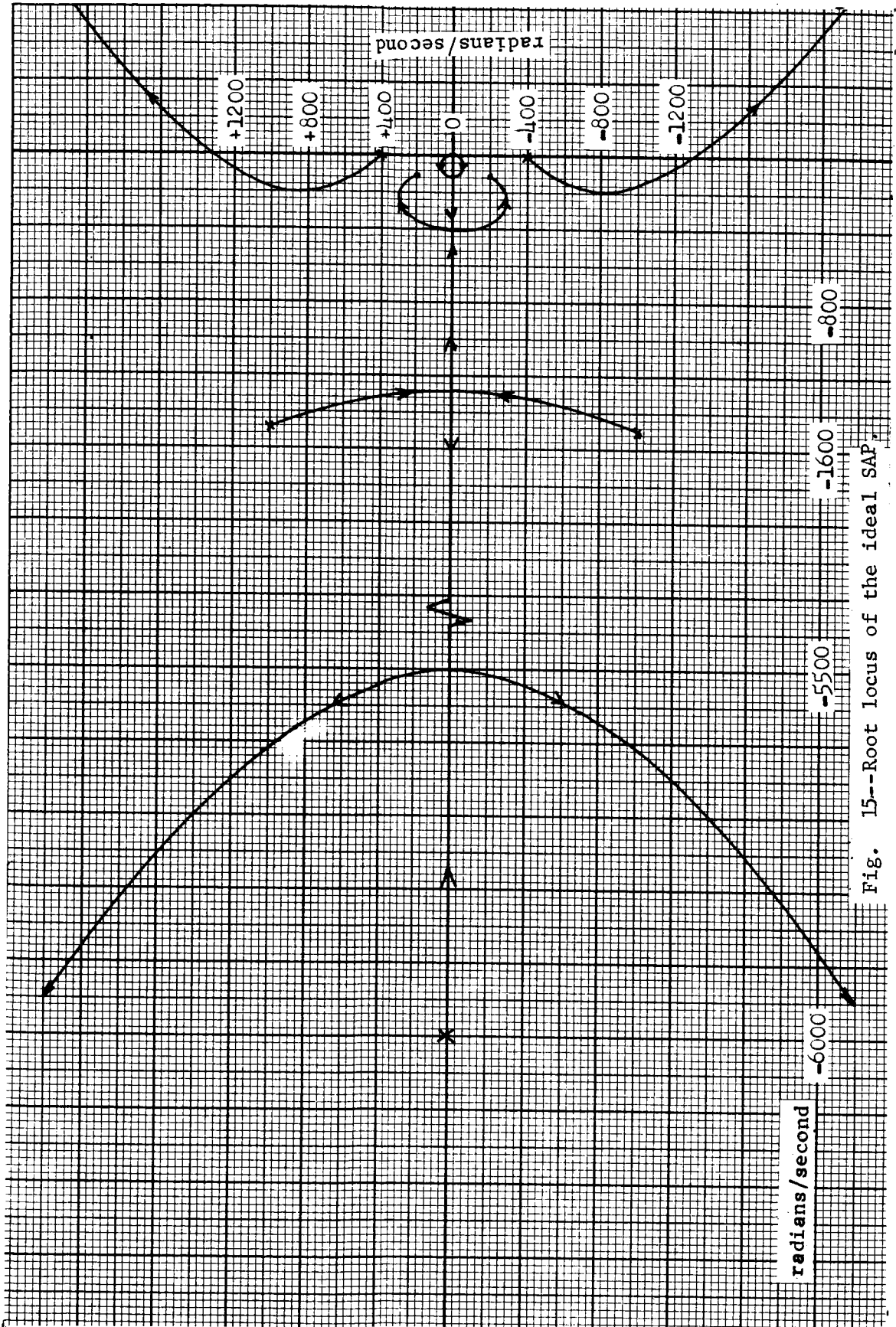


Fig. 15--Root locus of the ideal SAP.

$$\begin{aligned}
P_1 &= -66 + j43 , \\
P_2 &= -66 - j43 , \\
P_3 &= -813 , \\
P_4 &= -165 + j660 , \\
P_5 &= -165 - j660 , \\
P_6 &= -1805 ,
\end{aligned}
\tag{IV-6}$$

and

$$P_7 = -5923 .$$

The transfer function of the closed loop can be written as

$$\frac{\Theta_2(S)}{L_{yge}(S)} = \frac{6.28 \times 10^{-2} (S+1)(S+6000)(S+1500+j1000)(S+1500-j1000)}{\prod_{i=1}^{i=7} (S-P_i)} ,
\tag{IV-7}$$

where the P_i 's are given in (IV-6).

A Bode plot of the open-loop transfer function $KG(S)H(S)$ for $K = 10 \times 10^{12}$ is shown in Fig. 16. The relative stability of the closed-loop SAP, as indicated by the root locus plot, is confirmed by a gain margin of 10.0 decibels and a phase margin of 25 degrees in Fig. 16.

C. Stability of an Ideal SAP with Finite Torsional Stiffness of the Gas Bearing

Analysis of the signal flow graph of the floated gimballed gyroscope in Fig. 11 yields the following transfer function relating

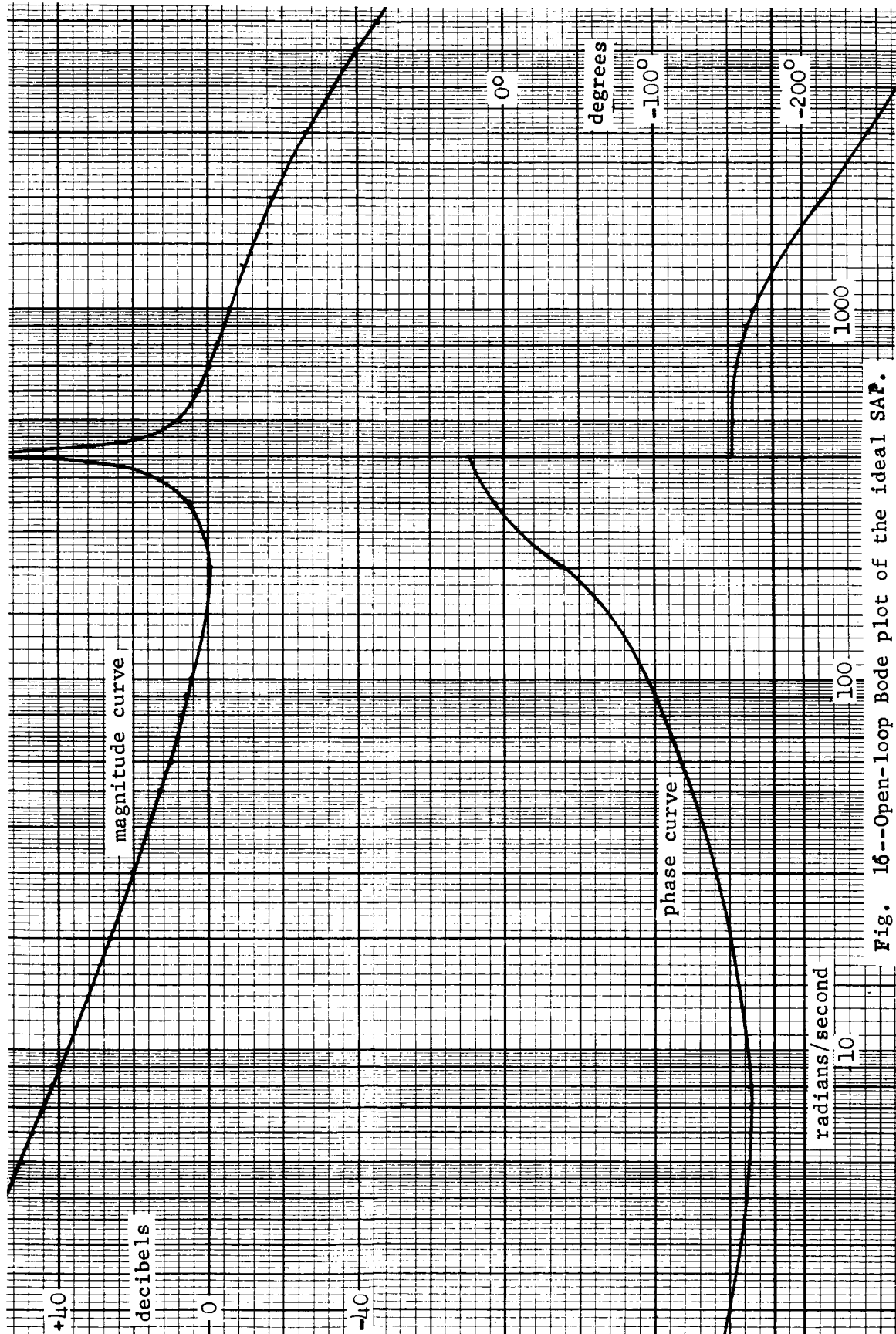


Fig. 16--Open-loop Bode plot of the ideal SAP.

the Laplace Transform of the error angle θ_2 , to the Laplace Transform of the applied torque L_{yg} :

$$K_1 G(S) = \frac{\theta_2(S)}{L_{yg}(S)} = \frac{\frac{1}{H_W}}{S \left\{ \frac{I_{yf} I_{zf} I_{yg}}{H_W^2 K_b} S^4 + \left(\frac{I_{yg}}{K_b} + \frac{I_{zf}(I_{yg} + I_{yf})}{H_W^2} \right) S^2 + 1 \right\}} \quad (IV-8)$$

Note that if K_b is allowed to approach infinity in (IV-8), the transfer function becomes the transfer function for an ideal SAP with infinite torsional stiffness in (IV-3). An analysis of (IV-8) indicates that the inclusion of finite torsional stiffness has introduced another pair of conjugate imaginary poles. The floated gimballed gyroscope with finite torsional stiffness of the gas bearing has five poles located on the $j\omega$ -axis.

In order to comprehend more fully the requirements for stability of an ideal SAP with finite torsional stiffness of the gas bearing, a particular set of numerical values will be used. The numerical values, which were obtained from information furnished by the Marshall Space Center in Huntsville, Alabama, are

$$\begin{aligned} H_W &= 2.51 \times 10^6 \text{ gm cm}^2 / \text{sec}, \\ I_{zf} &= 1195 \text{ gm cm}^2, \\ I_{yf} &= 1565 \text{ gm cm}^2, \\ I_{yg} &= 18380 \text{ gm cm}^2, \end{aligned} \quad (IV-9)$$

and

$$K_b = 7.0 \times 10^9 \text{ dyne cm/radian.}$$

Substituting (IV-9) into (IV-8) gives the transfer function of the floated gimballed gyroscope:

$$K_1 G(S) = \frac{5.1 \times 10^5}{S[S^2 + (400)^2][S^2 + (2840)^2]} \quad (\text{IV-10})$$

The root locus plot of the characteristic equation of (IV-1), with $K_1 G(S)$ from (IV-10) and $K_2 H(S)$ from (IV-2), for variations of the gain $K = K_1 K_2$, is shown in Fig. 17. A gain of 10×10^{12} will furnish good stability with the closed-loop poles located in the S-plane at

$$\begin{aligned} P_1 &= -66 + j43 , \\ P_2 &= -66 - j43 , \\ P_3 &= -813 , \\ P_4 &= -165 + j660 , \\ P_5 &= -165 - j660 , \\ P_6 &= -1805 , \\ P_7 &= -5923 , \\ P_8 &= -120 + j2800 , \end{aligned} \quad (\text{IV-11})$$

and

$$P_9 = -120 - j2800 .$$

The transfer function of the closed loop can be written as

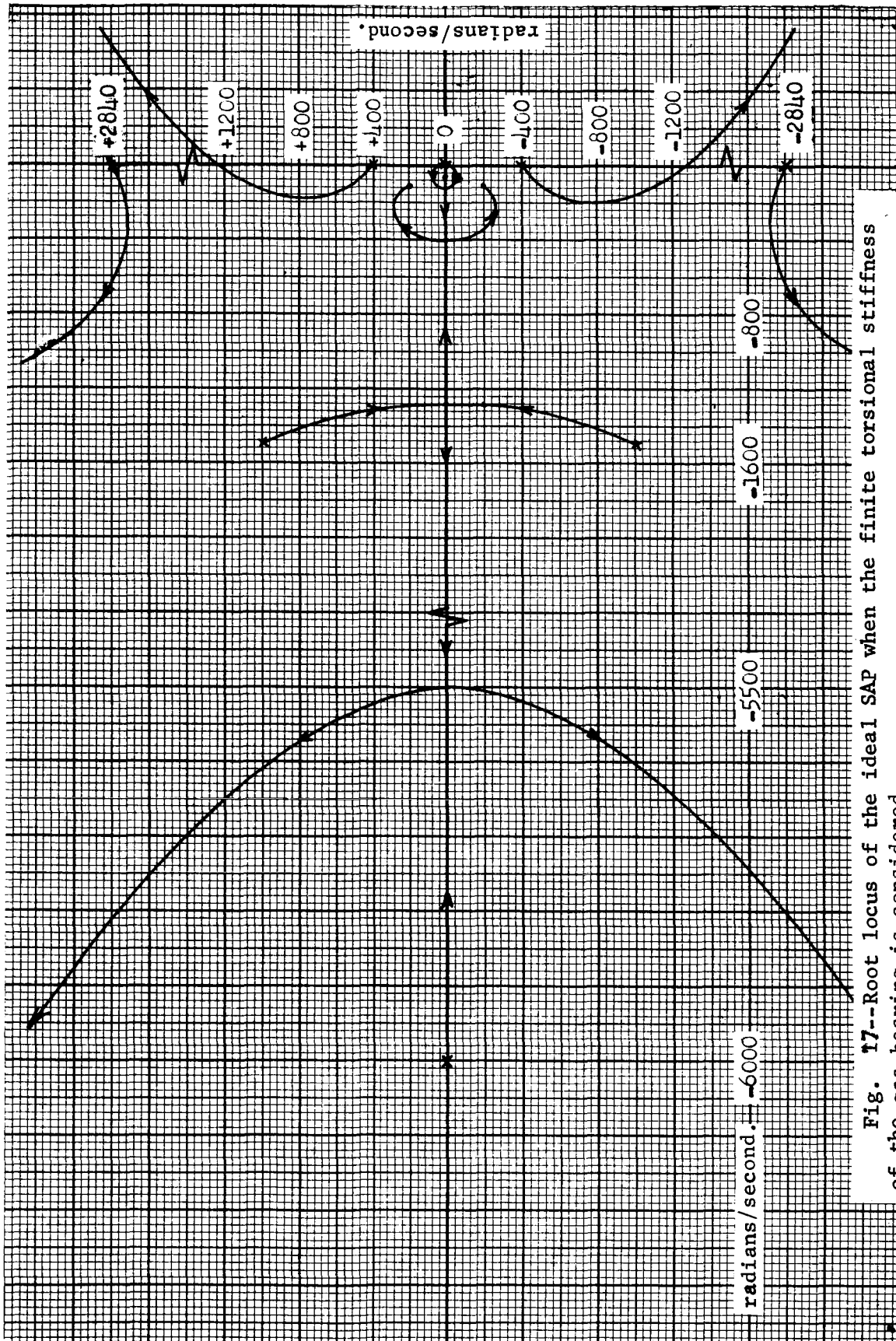


Fig. 17--Root locus of the ideal SAP when the finite torsional stiffness of the gas bearing is considered.

$$\frac{\Theta_2(s)}{L_{yge}(s)} = \frac{5.1 \times 10^5 \left\{ (s+1)(s+6000)(s+1500+j1000)(s+1500-j1000) \right\}}{\prod_{i=1}^{i=9} (s - P_i)}, \quad (IV-12)$$

where the P_i 's are given in (IV-11).

V. ANALYSIS OF AN IDEAL SAP [8,9]

A. Introduction

The equations of motion of an ideal SAP contain the sine and cosine of the dependent variable θ_1 . The presence of these trigonometric terms makes the equations of motion non-linear, if the input contains ω_{xc} or ω_{zc} . This necessitates the use of either digital or analog simulation when the inputs ω_{xc} and ω_{zc} are present. However, other inputs to the system can be analyzed, when ω_{xc} and ω_{zc} are zero, since the equations governing the motion of the SAP for these inputs are linear differential equations. Section B of this chapter will be concerned with the transfer functions of an ideal SAP that relate the output θ_1 to the inputs ω_{yc} , L_{yge} , and L_{zf} , when ω_{xc} and ω_{zc} are zero. In section C of this chapter, ω_{zg} will be treated as an input and the transfer functions relating θ_1 and θ_2 to ω_{zg} will be derived with all other inputs being zero. Actually, ω_{zg} is the sum of $\omega_{xc} \sin \theta_1$ and $\omega_{zc} \cos \theta_1$, which can be assumed to be independent of θ_1 if the variations in θ_1 are small. Under the conditions of small variation of θ_1 and all inputs zero except ω_{zg} , the transfer functions relating θ_1 and θ_2 to ω_{zg} have physical meaning. The evaluation of θ_1 and θ_2 for a step input of ω_{zg} will provide useful information concerning the ability of the ideal SAP to react to input angular rates of the case that are perpendicular to the reference axis. Only the

equations of an ideal SAP with infinite torsional stiffness of the gas bearing will be considered in this chapter.

B. Transfer Functions of an Ideal
SAP with Infinite Torsional Stiffness
of the Gas Bearing

Analysis of the signal flow graph in Fig. 8 or the block diagram in Fig. 9 will yield the following transfer functions:

$$\frac{\theta_1(s)}{\omega_{yc}(s)} = -\frac{1}{s}, \quad (V-1)$$

$$\frac{\theta_1(s)}{L_{yge}(s)} = \frac{1}{I_{yg} + I_{yf}} \cdot \frac{D(H)}{\prod (s - p_i)}, \quad (V-2)$$

and

$$\frac{\theta_1(s)}{L_{zfc}(s)} = \frac{-1}{I_{zf}(I_{yg} + I_{yf})} \cdot \frac{s H_w D(H) + K_2 N(H)}{s \prod (s - p_i)}, \quad (V-3)$$

where the p_i 's are the roots of $1 + KG(s) H(s) = 0$, and $N(H)$ and $D(H)$ are the numerator and denominator polynomials of $H(s)$, respectively. Each transfer function was derived by assuming all inputs zero, except the input of interest. Since the equations of motion, with ω_{xc} and ω_{zc} zero, are linear differential equations, superposition will hold, and (V-1), (V-2) and V-3) can be combined to give

$$\theta_1(s) = \frac{\omega_{yc}(s)}{s} + \frac{1}{I_{yg} + I_{yf}} \left\{ \frac{L_{yge}(s) D(H) - \frac{L_{zf}(s) H_w D(H)}{I_{zf}} - \frac{L_{zf}(s) K_2 N(H)}{s I_{zf}}}{\prod (s-p_i)} \right\} \quad (V-4)$$

For the numerical values used in chapter IV and the $H(s)$ in (II-3) with $K = 10 \times 10^{12}$, the transfer function in (V-1), (V-2) and (V-3) become:

$$\frac{\theta_1(s)}{\omega_{yc}(s)} = -\frac{1}{s} \quad (V-5)$$

$$\frac{\theta_1(s)}{L_{yge}(s)} = \frac{5 \times 10^{-5} (s+1)(s+6000)(s+1500+j1000)(s+1500-j1000)}{\prod_{i=1}^7 (s-p_i)} \quad (V-6)$$

$$\frac{\theta_1(s)}{L_{zf}(s)} = \frac{-6.28 \times 10^{-2} (s+1)(s+6000)(s+1500-j1000)(s+1500+j1000)}{\prod_{i=1}^7 (s-p_i)} - \frac{39.9 \times 10^5 (s+50)(s+100+j200)(s+100-j200)}{s \prod_{i=1}^7 (s-p_i)} \quad (V-7)$$

where

$$\begin{aligned} p_1 &= -66 + j43, \\ p_2 &= -66 - j43, \\ p_3 &= -813, \\ p_4 &= -165 + j660, \\ p_5 &= -165 - j660, \\ p_6 &= -1805, \\ \text{and } p_7 &= -5923, \end{aligned} \quad (V-8)$$

C. Reaction of the Ideal SAP to Angular Rates
Perpendicular to the Reference Axis

The ideal SAP must be capable of reacting to inputs ω_{xc} and ω_{zc} without appreciable change in the relative alignment of the float, gimbal, and case, with respect to each other. The ability of the ideal SAP to maintain this alignment can be investigated by treating $\omega_{zg} = \omega_{xc} \sin \theta_1 + \omega_{zc} \cos \theta_1$ as an input that is a known function of time while all other inputs are held at zero. If the variations in the angles θ_1 and θ_2 can be shown to be very small for a step input of ω_{zg} , the reference axis will move with the case for inputs ω_{xc} and ω_{zc} , thus maintaining the desired reference.

An analysis of the signal flow graph in Fig. 8 or the block diagram in Fig. 9 will yield the following transfer functions:

$$\frac{\theta_1(s)}{\omega_{zg}(s)} = \frac{1}{I_{yg} + I_{yf}} \cdot \frac{K_2 N(H)}{\prod (s - p_i)} \quad (V-9)$$

and

$$\frac{\theta_2(s)}{\omega_{zg}(s)} = \frac{\left\{ s^2 + \frac{H_w^2}{I_{zf}(I_{yg} + I_{yf})} \right\} D(H)}{\prod (s - p_i)} \quad (V-10)$$

where the p_i 's are the roots of the characteristic equation

$1 + KG(s) H(s) = 0$, and $D(H)$ is the denominator polynomial of $H(s)$.

Substituting the numerical values from (IV-4) and the $H(S)$ from (IV-2) with $K=10 \times 10^{12}$ into (V-9) and (V-10) yields

$$\frac{\theta_1(S)}{\omega_{zg}(S)} = \frac{79.8 \times 10^8 (S+50)(S+100+j200)(S+100-j200)}{\prod_{i=1}^7 (S-p_i)} \quad (V-11)$$

and

$$\frac{\theta_2(S)}{\omega_{zg}(S)} = \frac{\{S^2 + (400)^2\} \{(S+1)(S+6000)(S+1500+j1000)(S+1500-j1000)\}}{\prod_{i=1}^7 (S-p_i)},$$

where the p_i 's are given in (V-8).

For a step input $\omega_{zg} = 0.1$ radians per second, $\theta_1(t)$ and $\theta_2(t)$ will reach a steady-state value in approximately 5/66 seconds. The steady-state values will be

$$\theta_{1SS} = 16 \text{ arc seconds}$$

and

$$\theta_{2SS} = 2.6 \text{ arc seconds.}$$

Therefore, the ideal SAP is capable of maintaining the desired reference alignment to a high degree of accuracy.

VI. CONCLUSION

According to (V-1), the angle between the case and the gimbal of an ideal SAP, θ_1 , for an input angular velocity of the case about the reference axis of the SAP, ω_{yc} , is

$$\theta_1 = - \int \omega_{yc} dt , \quad (VI-1)$$

where the reference direction for θ_1 is shown in Fig 5. Since the angle θ_1 is the output of an ideal SAP, an ideal SAP measures the integral of the angular velocity of its case about its reference axis. The actual value of θ_1 may differ from the integral of ω_{yc} due to input angular velocities perpendicular to the reference axis of the SAP or due to error torques developed inside the SAP. An indication as to the amount that θ_1 may vary from the integral of ω_{yc} can be obtained by assuming step disturbances for the inputs ω_{yc} , L_{yge} , ω_{zg} and L_{zfe} shown in Fig. 9. The solutions to (V-5), (V-6), (V-9), and (V-11) with step inputs of $\omega_{yc} = W_{yc} u(t)$, $L_{yge} = L_y u(t)$, $L_{zfe} = L_z u(t)$, and $\omega_{zg} = W_{zg} u(t)$ respectively, will combine to give

$$\begin{aligned} \theta_1(t) = & -W_{yc} t + 38.3 \times 10^{-15} L_y - 40.2 \times 10^{-8} t L_z - 49.4 \times 10^{-12} L_z \\ & + 80.4 \times 10^{-5} W_{zg} + \sum_{i=1}^7 K_i e^{P_i t} , \end{aligned}$$

(VI-2)

where the p_i 's are given in (V-8). The first term in (VI-2) is the desired output and the remaining terms are error terms. After 5/66 seconds the $\sum_{i=1}^k K_i e^{p_i t}$ terms are approximately zero. The second, fourth, and fifth terms are due to L_{yge} , L_{zfe} and ω_{gc} respectively and are small. The third term in (VI-2) could be appreciable unless the magnitude of the step error torque is very small, thus making it necessary to design the floated gimbaled gyroscope such that L_z is small.

Evaluation of (V-5) and (V-7) shows that the output $\theta_1(t)$ for inputs ω_{yc} and L_z can be written as

$$\theta_1(t) = - \int \omega_{yc} dt - 40.2 \times 10^{-8} \int L_z dt + E(t) \quad (VI-3)$$

If the center of mass of the wheel of the floated gimbaled gyroscope is shifted a small amount along its spin axis, a torque L_z will be introduced about the z-axis of the float proportional to any acceleration of the case along the reference axis. Equation (VI-3) would then become

$$\theta_1(t) = - \int \omega_{yc} dt - k \int \ddot{x}_c dt + E(t), \quad (VI-4)$$

where \ddot{x}_c is the acceleration of the case along the reference axis of the SAP and k is a constant. If $E(t)$ is small compared to the other terms in (VI-4), the output is the negative of the sum of a term proportional to the integral of the acceleration of the

case along its reference axis and the integral of ω_{yc} . Operating under these conditions the floated gimbaled gyroscope and feedback loop is a Pendulous Integrating Gyro Accelerometer (PIGA).

The consideration of finite torsional stiffness of the gas bearing, instead of infinite torsional stiffness, introduces two more complex poles in all of the transfer functions in Chapter V as well as changing the numerator of each. An analysis of Figs. 12 or 13 would readily yield these transfer function for the ideal SAP when finite torsion stiffness of the gas bearing is considered.

The block diagram in Fig. 9 and 13 for the ideal SAP with finite and infinite torsional stiffness of the gas bearing, respectively, can be used to simulate on either digital or analog equipment the actual motion of the ideal SAP.

REFERENCES

1. William V. Houston, Principles of Mathematical Physics, McGraw-Hill Book Company, New York, 1948.
2. Richard Kolk, Modern Flight Dynamics, Prentice-Hall, Inc., Englewood, New Jersey, 1960.
3. James L. Lowry, An Introduction to Analytic Platforms for Inertial Guidance, Technical Report, Contract NAS8-20004, Auburn University, Auburn, Alabama, April 1966.
4. Herbert Goldstein, Classical Mechanics, Addison-Wesley Publishing Company, Inc., Reading, Massachusetts, 1959.
5. George B. Doane III, A Capsule Summary of Rigid Body Dynamics Applicable to Gyro Investigation, R-ASTR-G-WP-39-64.
6. George B. Doane III, The Effect of Gas Supply Pressure on the Gyro/Accelerometer Servosystem Dynamics, R-ASTR-G-WP-5-65.
7. George B. Doane III, Further Considerations on the Dynamic Effects of Finite Torsional Stiffness in Gyroscopic Instruments, R-ASTR-G-WP-18-65.
8. Charles H. Wilts, Principles of Feedback Control, Addison-Wesley Publishing Company, Inc., Reading, Massachusetts, 1960.
9. John J. D'Azzp and Constantine H. Houpis, Feedback Control System Analysis and Synthesis, McGraw-Hill Book Company, New York, 1966.